NAVAL POSTGRADUATE SCHOOL
Monterey, California

THESIS

MODELING OF JET VANE HEAT-TRANSFER
CHARACTERISTICS AND SIMULATION
OF THERMAL RESPONSE

by

Mark A. Hatzenbuehler

June 1988

Thesis Advisor: R. H. Nunn

SECURITY CLASSIFICATION OF THIS PAGE

REPORT DOCUMENTATION PAGE

1a REPORT SECURITY CLASSIFICATION UNCLASSIFIED	1b RESTRICTIVE MARKINGS
2a SECURITY CLASSIFICATION AUTHORITY	3 DISTRIBUTION/AVAILABILITY OF REPORT Approved for public release, distribution is unlimited.
2b DECLASSIFICATION/DOWNGRADING SCHEDULE	
4 PERFORMING ORGANIZATION REPORT NUMBER(S)	5 MONITORING ORGANIZATION REPORT NUMBER(S)
6a NAME OF PERFORMING ORGANIZATION Naval Postgraduate School 6b OFFICE SYMBOL (If applicable) Code 69	7a NAME OF MONITORING ORGANIZATION Naval Postgraduate School
6c ADDRESS (City, State, and ZIP Code) Monterey, California 93943-5000	7b ADDRESS (City, State, and ZIP Code) Monterey, California 93943-5000
8a NAME OF FUNDING/SPONSORING ORGANIZATION 8b OFFICE SYMBOL (If applicable)	9 PROCUREMENT INSTRUMENT IDENTIFICATION NUMBER
8c ADDRESS (City, State, and ZIP Code)	10 SOURCE OF FUNDING NUMBERS PROGRAM ELEMENT NO / PROJECT NO / TASK NO / WORK UNIT ACCESSION NO

11 TITLE (Include Security Classification)
Modeling of Jet Vane Heat-Transfer Characteristics and Simulation of Thermal Response

12 PERSONAL AUTHOR(S)

13a TYPE OF REPORT Master's Thesis	13b TIME COVERED FROM _____ TO _____	14 DATE OF REPORT (Year, Month, Day) 1988, June	15 PAGE COUNT 92

16 SUPPLEMENTARY NOTATION
The views expressed in this thesis are those of the author and do not reflect the official policy or position of the Department of Defense or the U. S. Government.

17 COSATI CODES		
FIELD	GROUP	SUB-GROUP

18 SUBJECT TERMS (Continue on reverse if necessary and identify by block number)
Dynamic Systems Modeling; Model Simulation, Thermal Response; Parametric System Identification, Theses.

19 ABSTRACT (Continue on reverse if necessary and identify by block number)

The development of a dynamic computational model capable of predicting, with the requisite design certainty, the transient thermal response of jet vane thrust control systems has been undertaken. The modeling and simulation procedures utilized are based on the concept that the thermal processes associated with jet vane operation can be put into a transfer function form commonly found in the discipline of automatic controls. Well established system identification methods are employed to formulate and verify the relationships between the various gains and frequencies of the transfer function model and experimental data, provided by Naval Weapons Center, China Lake.

Keywords:

20 DISTRIBUTION/AVAILABILITY OF ABSTRACT ☒ UNCLASSIFIED/UNLIMITED ☐ SAME AS RPT ☐ DTIC USERS	21 ABSTRACT SECURITY CLASSIFICATION UNCLASSIFIED
22a NAME OF RESPONSIBLE INDIVIDUAL Professor R. H. Nunn	22b TELEPHONE (Include Area Code) (408)646-2365 22c OFFICE SYMBOL 69Nn

DD FORM 1473, 84 MAR 83 APR edition may be used until exhausted
All other editions are obsolete

SECURITY CLASSIFICATION OF THIS PAGE

U.S. Government Printing Office: 1986—606-243

UNCLASSIFIED

Approved for public release; distribution unlimited

MODELING OF JET VANE HEAT-TRANSFER CHARACTERISTICS AND SIMULATION OF THERMAL RESPONSE

Mark A. Hatzenbuehler
Lieutenant, United States Navy
B.S, University of Texas, 1980

Submitted in partial fulfillment of the
requirements for the degree of

MASTER OF SCIENCE IN MECHANICAL ENGINEERING

from

NAVAL POSTGRADUATE SCHOOL
June 1988

Author: _____
Mark A. Hatzenbuehler

Approved by: _____
R. H. Nunn, Thesis Advisor

_____
A. J. Healey, Chairman
Department of Mechanical Engineering

_____
Gordon E. Schacher
Dean of Science and Engineering

ABSTRACT

The development of dynamic computational model capable of predicting, with the requisite design certainty, the transient thermal response of jet vane thrust control systems has been undertaken. The modeling and simulation procedures utilized are based on the concept that the thermal processes associated with jet vane operation can be put into a transfer function form commonly found in the discipline of automatic controls. Well established system identification methods are employed to formulate and verify the relationship between the various gains and frequencies of the transfer function model and experimental data provided by Naval Weapons Center, China Lake.

TABLE OF CONTENTS

LIST OF FIGURES

ACKNOWLEDGMENTS

I wish to express my heartfelt thanks to my thesis advisor, Professor Robert H. Nunn for his expert guidance and unfailing support throughout the course of this study. I am deeply grateful for having had the good fortune of working with a man of his patience and understanding.

I also want to thank my wife Sharon for her love, understanding and support through my entire Postgraduate Education.

I. INTRODUCTION

The demand for optimum maneuverability in the design of tactical missiles, as well as spacecraft launch vehicles, necessitates the application of active control systems. The control forces and momentum generated by such systems are essential to accomplish specified trajectory changes.

Of the various methods of active trajectory correction, thrust vector control (TVC) systems offer the only means of trajectory control that are independent of the external forces on the vehicle. Such capability is required when the flow past the vehicle's external aerodynamic surfaces (canards, wings, tails, etc.) is insufficient to generate the necessary control forces. This commonly occurs during low-speed flight, such as at launch or during hovering. High angle of attack flight may also lead to regimes where conventional aerodynamic lifting surfaces are inadequate [Ref. 1]. Furthermore, some design configurations render external control surfaces impractical, such as tube-launched missiles.

Three different methods of TVC have been developed and operationally tested: movable nozzle, secondary injection (internal fluid injection), and mechanical jet deflection systems [Refs. 2,3]. Comparison studies favor

the latter category which are characterized by relatively low actuation torques, rapid response and, in the case of a jet vane system, a small installation envelope. Of the various TVC systems, jet vanes have proven to be the most effective in delivering large thrust vector deflection angles (up to 30 degrees.) [Ref. 3]. They also offer the possibility of roll control and, for the case of a single exhaust nozzle arrangement, a jet vane device is the only practical system which could perform the task.

There are, however, disadvantages in the use of jet vane TVC. First, there are thrust losses on the order of 3-5% with the use of non-retractable vanes. In addition, the ability to achieve such high thrust deflection angles can result in axial trust losses proportional to 50 - 100% of the resulting side-force [Ref. 3]. Finally, the most significant problem with the use of jet vanes is the large thermal loading they experience during exposure to high temperature, supersonic, particulate-laden rocket exhaust gases. In the past, this problem has limited jet vanes to short duration use in engines with low temperature non-metalized propellants.

Jet vane TVC dates back more than 50 years to the rockets designed by R.H. Goddard, and has extended to Redstone, Sergent, Talos, Pershing, and Anglo II and III engines, as well as several installations in smaller tactical rockets [Refs. 1,2]. Due to the material problems

associated with the use of high energy aluminized propellents and the advance of other TVC systems, jet vane devices had been furthered studied only on a low level. New mission requirements, however, coupled with the above mentioned system capabilities have resulted in a renewed level of interest in the application of jet vane TVC especially for launch phase trajectory control.

The aerodynamic design of the jet vane can be performed with reasonable accuracy on the basis of supersonic flow theory with boundary layer corrections [Refs. 3,4]. It is significantly more difficult to calculate, with the same degree of certainty, the vane heat transfer characteristics due to its severe thermal environment. This inability to accurately predict jet vane transient thermal response results in design material selection and configuration based solely upon past experience and costly experimental findings.

Hence the development of a dynamic computational model capable of calculating, with the requisite design certainty, the transient thermal response of such systems would truly be beneficial. Such a model could provide a capacity for design optimization which is virtually non-existent in current design efforts.

II. BACKGROUND

The basic goal of jet vane heat transfer studies is to develop a capacity to accurately predict the transient thermal behavior of the vane. The severe thermal environment in which the vane operates makes analysis and modeling of the energy transport processes extremely difficult. A complete analysis would have to account for multi-phase, multi-component, three-dimensional and time dependent effects in the presence of shocks, boundary layer transition, and turbulence, separated flows, surface ablation, chemical reaction, solid-body and gaseous radiation [Ref. 5].

It can be assumed that all the details of the energy transport process will never be fully defined. The net effect of all the various complications mentioned above is to transfer energy to and from the vane system. This process causes energy flow within the vane which in turn results in a vane temperature distribution that varies with time.

This transient thermal response should reflect the nature of the surface heat transfer processes that drive it, as well as the thermal impact of various vane design parameters. Hence the transient response is the

"signature" of the combined effects of both the thermal environment and the vane construction [Ref. 5]. This concept is the basis for the modeling and simulation (M&S) study described herein.

The goal of the M&S study has been to develop a dynamic model of vane thermal behavior. A model that could predict, with sufficient accuracy, the transient thermal response of the vane would be an invaluable design tool. For instance it could be used to predict the effects of design changes without the need for costly experimentation and testing. Also, sub-scale test data could be used to predict the full scale jet vane response. Most significant is the model's inherent ability to easily accommodate design optimization. The model could be used for deductive purposes also. For example, measured vane temperature data could be used for parameter estimation. That is, use of the model to deduce what would have had to occur in order to obtain the measured results. Furthermore, estimation of local temperatures could be made at points in the vane where accessibility, sensor survivability and other conditions render measurement impractical if not impossible.

Research has shown that the traditional approach to modeling a system such as this would be to construct a comprehensive model that would treat the flow environment of the vane and the vane itself in fine numerical detail.

Numerical techniques such as finite-element analysis or the finite-difference method would then be employed to determine both the steady-state heat transfer and the temperature distribution. The M&S method can thus be considered a vast simplification of a conventional numerical model. A basic assumption of this method is that sufficient accuracy can be obtained if the flow and vane are considered to be made up of relatively few thermal components. An important facet of the M&S model is the computation of temperature distribution as a function of time. This transient response capability lends itself well to model verification based on actual test data.

The modeling procedures used in this study are based on the concept that the thermal processes associated with jet vane operation can in fact be put into a transfer-function form commonly found in the discipline of automatic controls. Hence, experimental data can be related to the various gains and frequencies of the transfer function by well established system identification methods. The establishment and verification of these relationships has been the objective of this study.

III. THERMAL MODELING APPROACH

A. CONCEPT

The modeling procedures used in this study, as previously mentioned, are based on the concept that the transient thermal response of a jet vane can be formulated by the use of transfer functions. These transfer functions are developed from equations defining the various heat transfer processes occurring during jet vane operation. The "lumped-heat-capacity" method is the analytical approach employed to develop such equations. This analysis yields reasonably good results when the resistance to heat transfer by conduction is small compared with the convective resistance at the surface. Hence, the non-dimensional Biot number (Bi) becomes a most significant system parameter. The Biot number denotes the resistance to conduction in the vane relative to the convective resistance of the rocket exhaust flow. Therefore, to ensure that the error resulting a lumped capacitance analysis is minimized, the following condition must be satisfied,

$$Bi = hV/KA < 0.1 \qquad (3.1)$$

where h is the heat transfer coefficient, K is the thermal conductivity and V and A are the volume and surface area respectively [Ref. 6:pp. 134-135].

B. METHODOLOGY

A jet vane of a particular design was hypothetically configured to consist of several discrete thermal parts or "lumps". Then a thermal circuit was constructed with nodes located at the center of mass of each lump. Figure 3.1 is a simplified, two lump, example of such a circuit.

As evidenced by Figure 3.1, thermal networks consist of only two types of components; thermal resistances (R) and thermal capacitances (C). The type of thermal resistance modeled depends on the mode of heat transfer being considered. For conduction between nodes,

$$R = L/KA \tag{3.2}$$

whereas for convection to the vane,

$$R = 1/hA \tag{3.3}$$

Similarly, there are resistances associated with radiation which is a subject treated in subsequent sections.

Thermal capacitance, on the other hand, is independent of the mode of heat transfer, and is defined as,

$$C = \rho V c_s \tag{3.4}$$

where ρ is the density of the vane material and c_s is the associated specific heat.

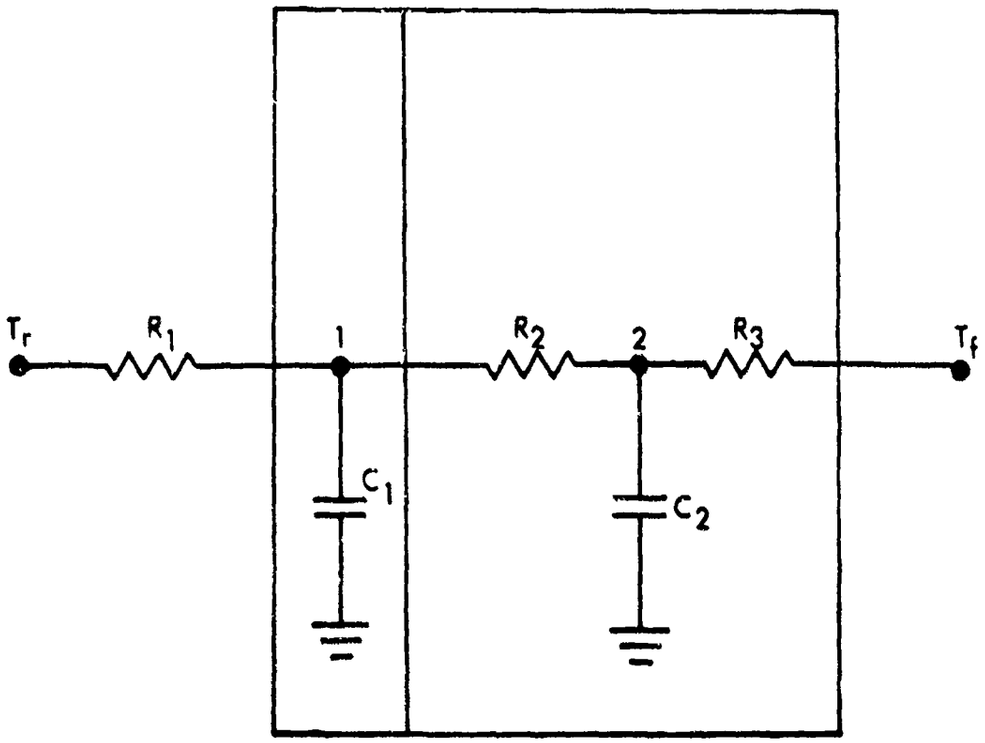

Figure 3.1 Two "lump" thermal circuit.

With the thermal network thus defined, the requisite governing equations are developed by means of an energy balance at each node. An energy balance is defined as follows:

Rate of heat flow into node.	=	Rate of heat flow out of node.	+	Rate of energy storage at a node.

For instance, a balance at node 1, of Figure 3.1, would yield:

$$\frac{T_r - T_1}{R_1} = \frac{T_1 - T_2}{R_2} + C_1 s T_1 \qquad (3.5)$$

where the letter s is the Laplace variable.

The nodal temperature can be expressed explicitly as follows:

$$T_1 = \frac{R_n}{1 + \tau s}\left[\frac{T_r}{R_1} + \frac{T_2}{R_2}\right] \qquad (3.6)$$

where,

$$\frac{1}{R_n} = \frac{1}{R_1} + \frac{1}{R_2} \qquad (3.7)$$

and the nodal time constant is given by

$$\tau = R_n C_1 \qquad (3.8)$$

A heat balance at node 2 would yield similar results, thereby providing sufficient information to determine both nodal temperatures as a function of time.

The computational method and the results of the application of the modeling approach outlined above are described in later sections.

C. APPLICATION

The modeling approach described above can be applied to various TVC jet vane configurations. In this study, however, a single design was used as the basis for all models. The particular design chosen was the retractable jet vane employed in the Stowable Three-Axis Reaction Steering (STARS) System, Figure 3.2, currently under development at the Naval Weapons Center (NWC), China Lake [Ref. 7]

The STARS jet vane is constructed of copper impregnated tungsten (10%Cu/W), comprised of 10% copper and 90% tungsten (by volume), and the vane support hardware is steel. A major operational feature of the STARS system is the variable positioning of the TVC vanes relative to the radial plane of the rocket nozzle exit. The TVC vane control system currently being tested is capable of moving the vanes from the fully inserted "active" position, to the fully retracted "stowed" position as illustrated in Figure 3.3. It should be noted, however, that all the analyses performed in this report were based solely on the TVC vane remaining in the "active" position.

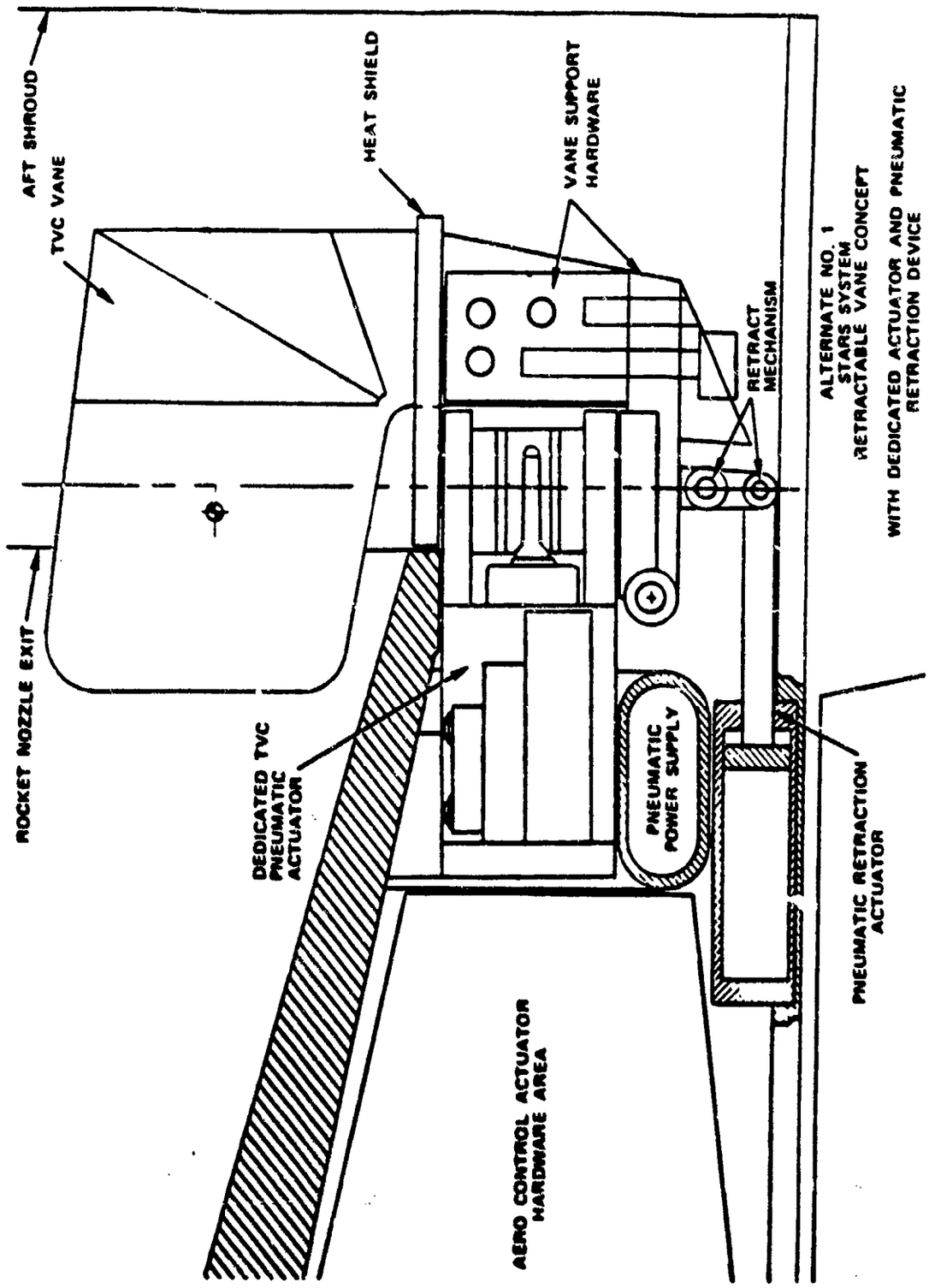

Figure 3.2 STARS TVC system concept.

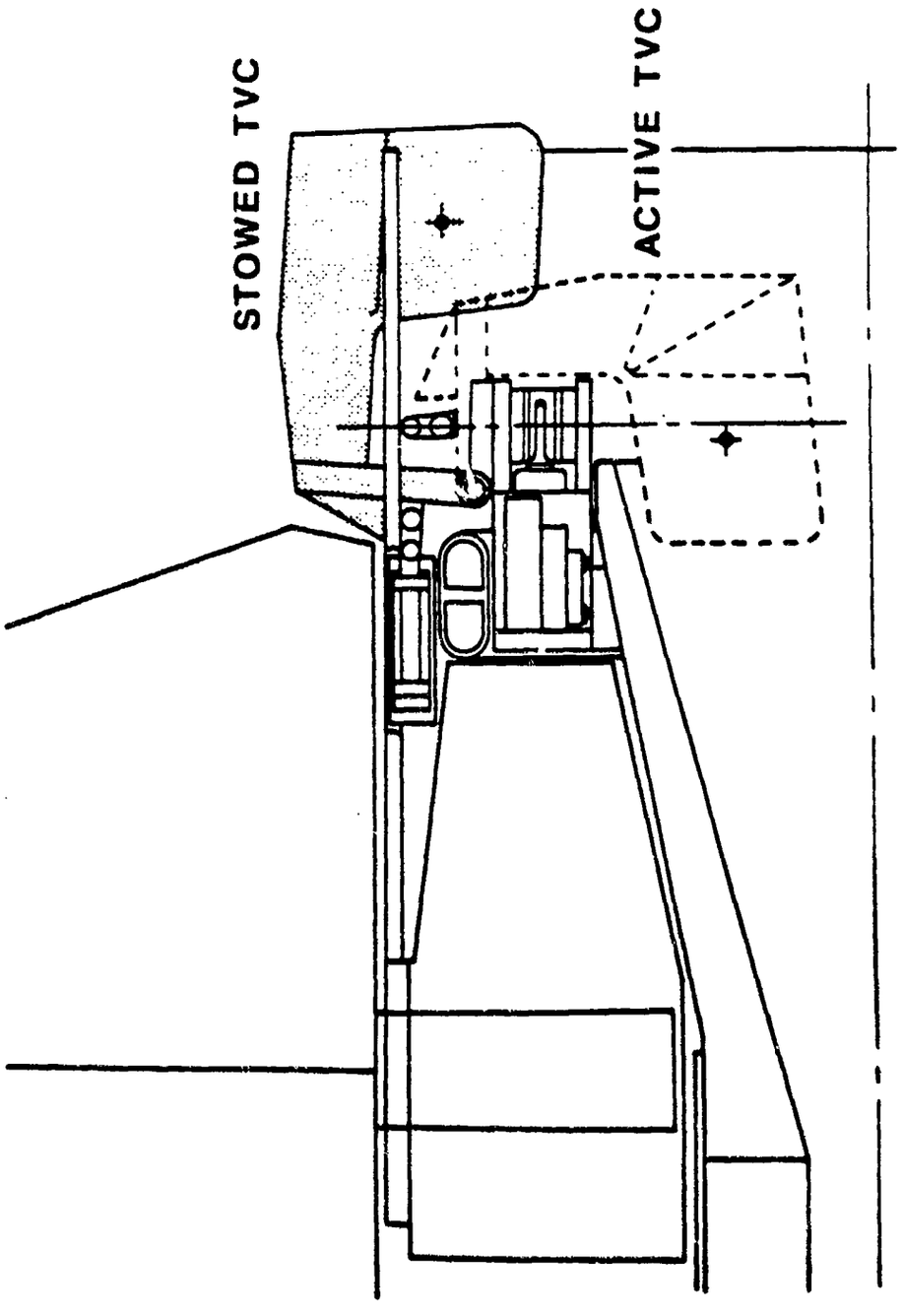

Figure 3.3. STARS TVC Stowage Concept

Figure 3.4 shows a single, full-scale TVC jet vane mounted on a mock-up of a Vertical Launch Modular Booster (VLMB) rocket motor and nozzle assembly. Figures 3.5 and 3.6 are used to demonstrate the TVC vane in the actual "stowed" and "active" positions respectively.

Figure 3.4 TVC Jet Vane Prototype

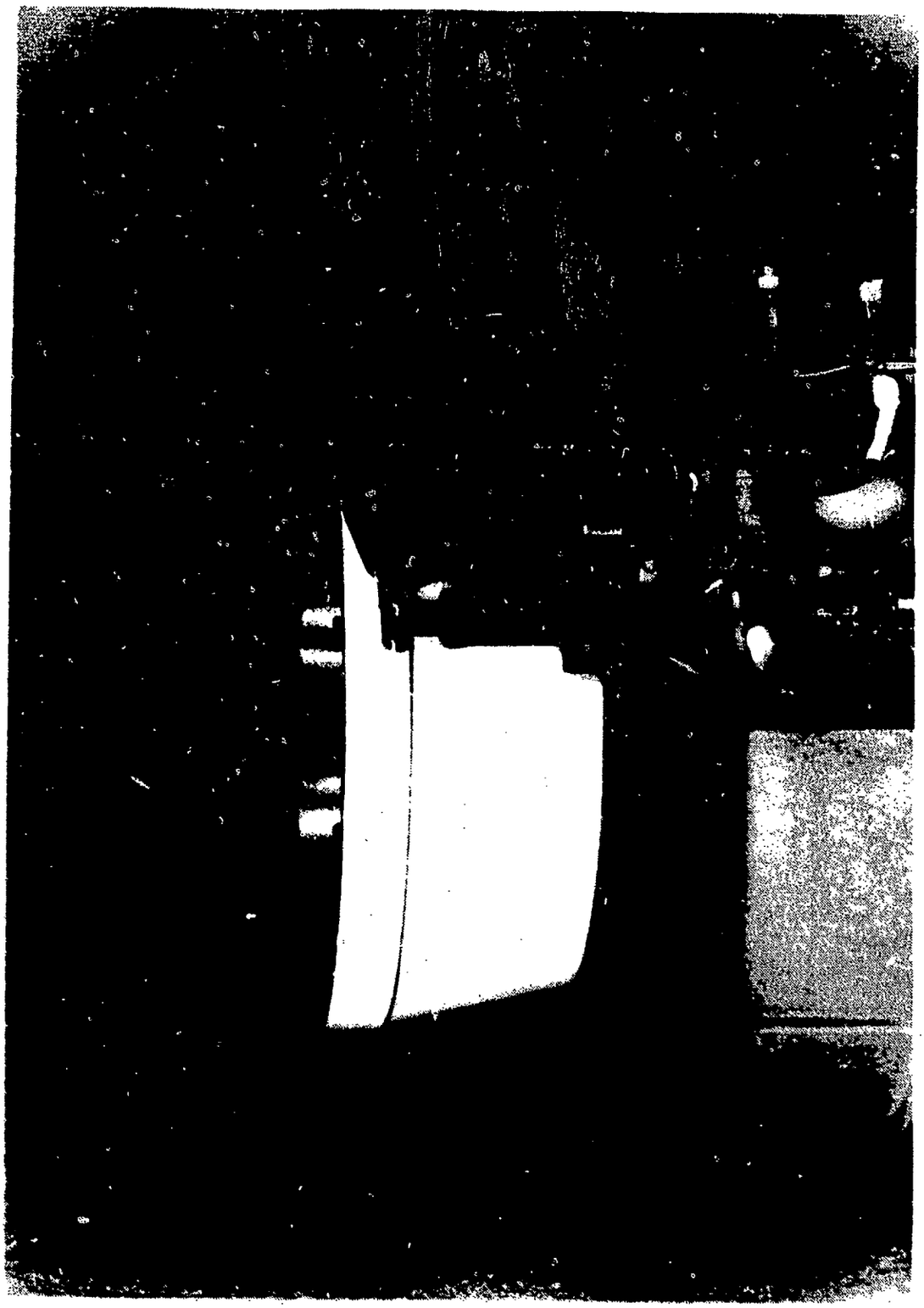

Figure 3.5 TVC Vane in the "Stowed" Position

Figure 3.6 TVC Vane in the "Active" Position

IV. MODEL DEVELOPMENT

A. BASIC DESCRIPTION

Investigations into the feasibility of applying the M&S approach to determine the dynamic thermal characteristics of the STARS jet vane system began in early 1986 [Ref. 5]. The results of these preliminary studies, as outlined below, form the basis of the work reported earlier. The thermal model described in this chapter is but one product of these early investigations.

The current model considers only two thermal energy input processes: forced convection at the vane surface and stagnation-point heat transfer at the leading edge. These processes are driven by the flow stagnation temperature which is a function of the rocket motor thrust levels. The basic assumption is that the stagnation temperature will follow the rise and fall of the thrust without a significant dynamic offset. Hence, the basic output of the model is a series of functions that give local vane temperatures as a function of thrust.

Several discretization schemes were tested and it was found that four "lumps" were sufficient to indicate the general thermal behavior of the vain. The four lumps are: the vain tip, vane body, shaft and mount.

B. GEOMETRICAL AND THERMAL ESTIMATIONS

In one step of the preliminary study the actual vane design was configured as a collection of lumps with regular geometries more suitable for calculating the thermal conduction properties. Figure 4.1 illustrates the actual vane geometry design while the discretized vane is shown in Figure 4.2 [Ref. 5]. The fictitious thermal vane was hypothesized as consisting of three rectangular solids: tip, fin and shaft. The tip was arbitrarily sized so as to have a chord length of 1.0% of the total vane chord of 3.75 inches. With the length fixed, the tip was shaped so as to have the same lateral area (chord x thickness) as that of the actual geometry. The discretized tip was separately identified to account for the stagnation properties of the convection heat transfer near the vane leading edge.

The remaining portion of the discretized fin was assumed to be subjected to thermal convection of a turbulent boundary layer type. This section was lumped into a rectangular solid of thickness equal to the average value of the tapered fin minus the tip and a span equal to the span of the actual fin.

The remaining length dimension was established by equating the volume of the rectangular solid to that of the actual fin (with tip removed). The vane shaft was similarly modeled into a rectangular solid, and assumed to be subjected to conduction heat transfer only.

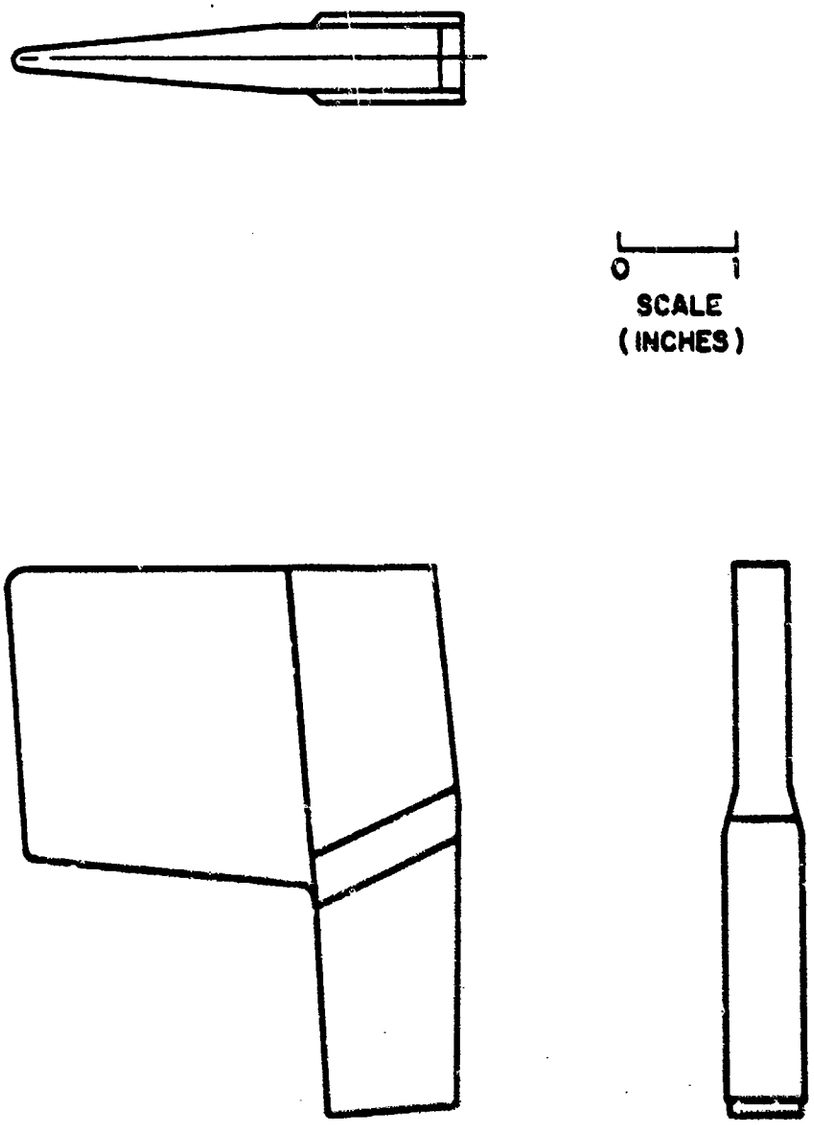

Figure 4.1. TVC Jet Vane Configuration

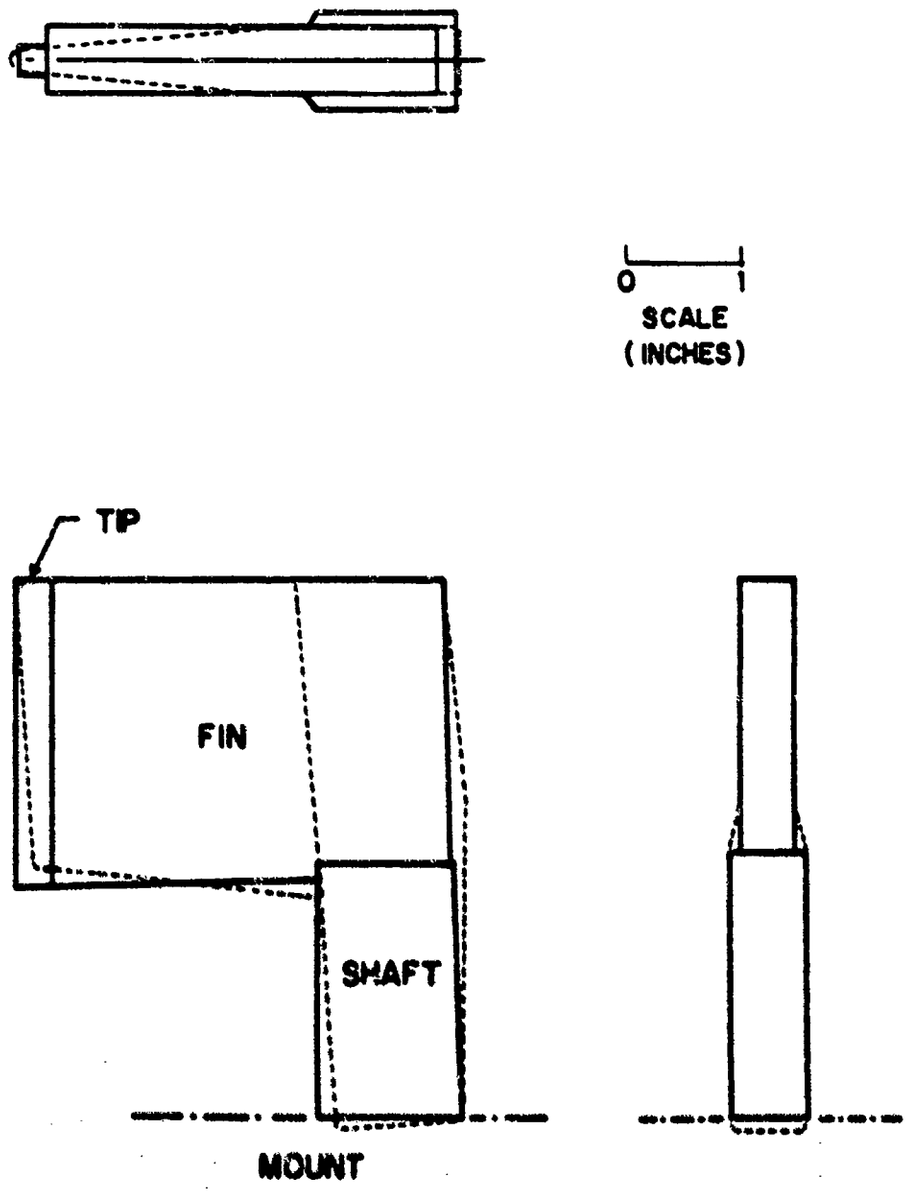

Figure 4.2. Discretized Version of TVC Jet Vane

The vane support mount, as shown in figure 3.2, is a relatively complex structure. In order to pursue the basic feasibility of the M&S method [Ref. 5], no attempt was made to model the thermal resistance of this component in detail. Instead, the conduction length and cross-section for the main mount components were estimated using a rough scalling procedure. An appropriate thermal resistance for the mount was then computed from an analysis of the analogous electrical circuit. In the preliminary studies the mount thermal resistance was used as an "adjustable parameter" in seeking agreement with the available experimental data. Hence, the determination of the correct value for the mount thermal resistance is one of the goals of the system identification procedure described in later chapters.

A thermal node was located at the center of mass of each of the components described above. These nodes are assumed to be the location of the energy storage associated with the entire mass. The thermal capacity of the mount was considered to be infinite, thus allowing its nodal temperature to remain constant at ambient temperature (ground) during the simulation.

It should be noted that the primary goal of the discretization process was to obtain adequate agreement with test results using the minimum number of thermal components.

This logic leads to the necessary simplicity that is key to the M&S approach and the results to be described later justify the development of such "simple" models.

C. DEVELOPMENT OF THE GOVERNING EQUATIONS

Applying the methodology described in the previous chapter to the discretization process outlined above yields thermal model illustrated in Figure 4.3. The nominal values of the various thermal components listed in the figure, were developed in the preliminary studies of Reference [8]. The governing equations can thus be formulated by using the energy balance technique of Chapter 3. For instance, for the tip node (node 1):

$$\frac{T_{R1} - T_1}{R_{F1}} = \frac{T_1 - T_i}{R_{1i}} + C_{1s}T_1 \qquad (4.1)$$

Here R_{F1} denotes the thermal resistance for convection to the fin, whereas, R_{1i} denotes the thermal resistance for conduction between nodes. The letters C and s represent thermal capacitance and the Laplace variable, respectively. T_{R2} and T_{R1} are the recovery temperatures.

The temperature at node 1 can therefore be expressed in terms of the adjacent nodal temperatures as follows:

$$T_1 = \frac{R_{N1}}{1+\tau_1 s}\left[\frac{T_{R1}}{R_{F1}} + \frac{T_i}{R_{1i}}\right] \qquad (4.2)$$

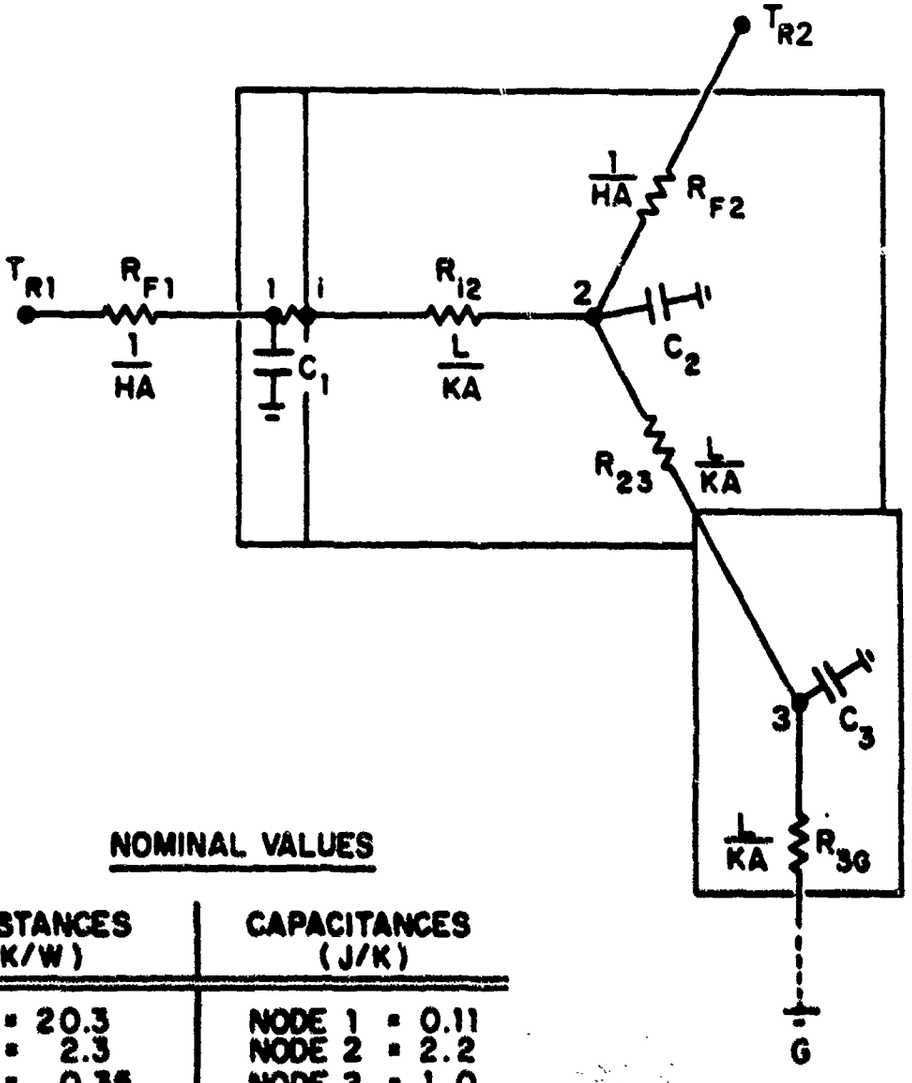

NOMINAL VALUES

RESISTANCES (K/W)	CAPACITANCES (J/K)
F1 = 20.3	NODE 1 = 0.11
F2 = 2.3	NODE 2 = 2.2
1i = 0.35	NODE 3 = 1.0
i2 = 1.6	
23 = 2.6	
3G = 10.3	

Figure 4.3. Nodal Configuration and Table of Estimated Values

where R_{N1} is given by:

$$\frac{1}{R_{N1}} = \frac{1}{R_{F1}} + \frac{1}{R_{1i}} \qquad (4.3)$$

and the nodal time constant is given by:

$$\tau_1 = R_{N1}C_1 \qquad (4.4)$$

Subsequent energy balances at each of the remaining nodes yields similar results, thereby providing sufficient information to determine each nodal temperature as a function of time. These nodal relationships are as follows:

$$T_2 = \frac{R_{N2}}{1+\tau_2 s}\left[\frac{T_{R2}}{R_{F2}} + \frac{T_i}{R_{i2}} + \frac{T_3}{R_{23}}\right] \qquad (4.5)$$

where, $\frac{1}{R_{N2}} = \frac{1}{R_{F2}} + \frac{1}{R_{i2}} + \frac{1}{R_{23}}$, and $\tau_2 = R_{N2}C_2$.

$$T_3 = \frac{R_{N3}}{1+\tau_3 s}\left[\frac{T_2}{R_{23}} + \frac{T_g}{R_{3g}}\right] \qquad (4.6)$$

where, $\frac{1}{R_{N3}} = \frac{1}{R_{23}} + \frac{1}{R_{3g}}$, and $\tau_3 = R_{N3}C_3$.

Initially, the entire system is assumed to be at thermal equilibrium such that all nodal temperatures are equal to the ambient temperature (ground) of the environment. The firing of the rocket motor disturbs this equilibrium and the subsequent changes in the two recovery temperatures provide

the inputs to the resulting heat transfer process. The development of these thermal inputs as a function of the rocket motor thrust levels is discussed in the next chapter.

V. ESTIMATES OF HEAT TRANSFER PARAMETERS

A. GENERAL DISCUSSION

As described in the previous chapter, only two inputs are required to drive the thermal model as presently configured. These forcing functions are the result of the heating occurring at the vane tip and along the downstream surface of the vane. It should be noted that the cooling effects of radiation and ablation, both important in the actual situation, are not yet addressed at this point in the study.

Estimates of the various heat transfer parameters presented in this chapter are, in large part, the result of extensive research previously conducted [Ref. 8]. Most of the computations performed in these preliminary studies were derived from analytical methods typically employed in the study turbulent flows and rocket engine heat transfer [Refs. 9,10].

B. THE PRANDTL NUMBER

A significant feature of high speed rocket exhaust flow is the large difference in temperature the gas experiences in decelerating near the body surface. Hence, it is necessary to account for the temperature dependency of the gas properties. In such cases both viscosity and

thermal conductivity are considered to vary significantly with temperature. The Prandtl number and specific heat, on the other hand, are considered constant inasmuch as their variations with temperature are of a lower order of magnitude than those of the other gas properties [Ref. 9: p. 304].

An important key to evaluating rocket engine heat transfer is the non-dimensional Prandtl number (Pr). The Prandtl number of the exhaust gas is derived from the viscosity (μ), the thermal conductivity (K), and the specific heat at constant pressure (C_p) as follows:

$$Pr = \frac{\mu C_p}{K} \tag{5.1}$$

Based on the above assumption that Pr and C_p are constant,

$$\frac{Pr}{C_p} = \frac{\mu}{K} = \text{constant} \tag{5.2}$$

and the thermal conductivity must vary in the same way as the viscosity. Thus an estimation of the gas viscosity leads to a thermal conductivity for a given Prandtl number and specific heat. A simple equation relating viscosity to thermal conductivity of the gas is

$$K = f\mu C_v \tag{5.3}$$

where C_v is the specific heat of the gas at constant volume and f is a constant. The Eucken formula [Ref. 10:p. 139] relates f with the ratio of specific heats (k) of the gas,

$$f = (9k-5)/4 \tag{5.4}$$

from which it follows that,

$$Pr = \frac{4k}{(9k-5)} \qquad (5.5)$$

which is the equation used in this work. If the specific gas constant (R_g) is given, the specific heat at a constant pressure is

$$C_p = \frac{R_g k}{(k-1)} \qquad (5.6)$$

Also used in this study is the standard power-law type formula [Ref. 11:p. 28] for determining viscosity,

$$\frac{\mu}{\mu_{ref}} = \left[\frac{T}{T_{ref}} \right] \qquad (5.7)$$

where n = 0.7 [Ref. 10:p. 8] and the reference viscosity has been taken to be $\mu = 4.0 \times 10^{-5}$ N-s/m^2 at $T_{ref} = 1000$ K.

C. STAGNATION POINT HEAT TRANSFER

In the analysis of stagnation point heating, the solution to the boundary layer equation requires the local fluid acceleration (ß) in the vicinity of that point be known. With supersonic flow, ß can be approximated based on the assumption that Newtonian flow prevails between the bow wave and the body [Ref. 9:p. 356]. An approximation for the local fluid acceleration has been derived by Nunn [Ref. 8: p. 18] and is given by:

$$ß = (du_\infty/dx)_{x=0} = (U/D)[8(P_\infty/P_{oy})(T_{o\infty}/T_\infty)]^{0.5} \qquad (5.8)$$

Here the subscript ($_\infty$) refers to freestream conditions, ($_o$) refers to stagnation conditions and ($_y$) denotes the conditions downstream of the normal shock. The pressure and temperature ratios in the above equation are known functions of the freestream Mach number.

The Stanton number (St) can be calculated from the following equation [Ref. 9:p. 366]:

$$St_o = 0.57(\beta D/U)^{0.5} Pr_o^{-0.6} Re_o^{-0.5} \qquad (5.9)$$

where β is defined above and Re is the Reynolds number.

D. TURBULENT BOUNDARY LAYER CONVECTION

The analysis of the heat transfer processes in high speed compressible flows is complicated by the fact that a considerable transfer of kinetic energy results from the deceleration occurring in the boundary layer. This results in temperatures within the boundary layer that are in excess of the freestream. As a result of this phenomenon the term "recovery temperature" (T_R) is introduced and is defined as the temperature that the surface will assume in the absence of heat transfer [Ref. 10:p. 14]. Thus the "recovery factor" (r) is defined as follows:

$$r = \frac{T_R - T_\infty}{T_o - T_\infty} \qquad (5.10)$$

It has been determined by Van Driest [Ref. 10:p. 14] and others that for a turbulent boundary, as is assumed here, recovery factor can be related to the Prandtl number by

$$r = Pr^{1/3} \tag{5.11}$$

A more-difficult problem arises from taking into account the gas property variation through the boundary layer as a function of temperature. Fortunately, for compressible flows, Eckert [Ref. 10:p. 8] provides a "reference temperature" (T_{ref}) for the boundary layer at which the various gas properties should be evaluated. Eckert's reference temperature as used in this study is calculated by

$$T_{ref} = 0.5T_{wall} + 0.28T_{\infty} + 0.27T_R \tag{5.12}$$

Initial calculations have been based upon the assumption that the wall temperature can be adequately represented by the mean of the recovery and ambient temperatures.

With T_{ref} thus defined, the gas viscosity and thermal conductivity can be estimated as described above. The Stanton number for turbulent, compressible flow is then given by [Ref. 10]:

$$St = 0.0296Pr^{-0.67}Re^{-0.2} \tag{5.13}$$

Nusselt numbers and thermal resistances can be calculated for the model nodes affected by stagnation and turbulent boundary layer heat transfer from the Stanton numbers discussed above.

Thermal resistances are also dependent upon associated dimensional parameters (length, area, volume), and as such, are scale dependent. For example, the stagnation point thermal resistance is proportional to $(\text{scale})^{-1.5}$, whereas the turbulent boundary layer thermal resistance decreases as $(\text{scale})^{-1.2}$. It should be noted that the simulations conducted in this study have been of a 1/4-scale model in order to seek a comparison with the 25% subscale test data provided by NWC.

E. INPUT REQUIREMENTS

In order to compute values for the thermal resistances, the stagnation temperature, stagnation pressure and Mach number of the freestream flow at the location of the jet vane must be determined. Therefore, inputs required for the simulation include the rocket motor chamber pressure, thrust and characteristic velocity along with the discharge coefficient and pressure ratio of the nozzle. The propellent gas properties must also be known. These include the gas molecular weight or specific gas constant and the ratio of specific heats.

Given the inputs mentioned above, the stagnation temperature can be determined by,

$$T_o = [C_d \; N \; c^*]^2 / R_g \qquad (5.14)$$

where,

C_d = nozzle discharge coefficient

$N = [k(2/k+1)^{(k+1)/(k-1)}]^{0.5}$

c^* = characteristic velocity

R_g = gas constant

k = ratio of specific heats

The Mach number at the nozzle exit is computed from

$$M_\infty^2 = [2/(k-1)]\,[(P_{O\infty}/P_\infty)^{(k-1)/k} - 1] \qquad (5.15)$$

where $P_{O\infty}/P_\infty$ is the nozzle pressure ratio. It should noted, that in this study, the Mach number at the nozzle exit is assumed to be that at the vane.

VI. PRELIMINARY RESULTS

A. COMPUTATIONAL MODEL

As part of the preliminary study described in Reference 5, a computer program has been written which coded the 3-NODE model and governing equations described in chapter IV, in the Dynamic Simulation Language (DSL). Details of this FORTRAN-based language are included in Reference 12. The simulation code is written such that the driving input is the rocket motor thrust. The thrust-time profile is approximated by a ramp from zero to a maximum in a period of 0.5s, held at this plateau for 2.5s, and ramped back to zero thrust over an additional 0.5s period. The thrust profile input used in the simulation described below is illustrated in Figure 6.1.

The magnitude of the convective heat transfer resistances, R_{F1} and R_{F2} are a function of flow part the vane [see Figure 4.3]. These resistances are very large prior to ignition and during burnout and are minimum during the period of maximum thrust. Modeling of this behavior is accomplished by varying the film coefficient according to the thrust schedule. These coefficients begin and end at 1% of the full flow value corresponding to the maximum thrust plateau.

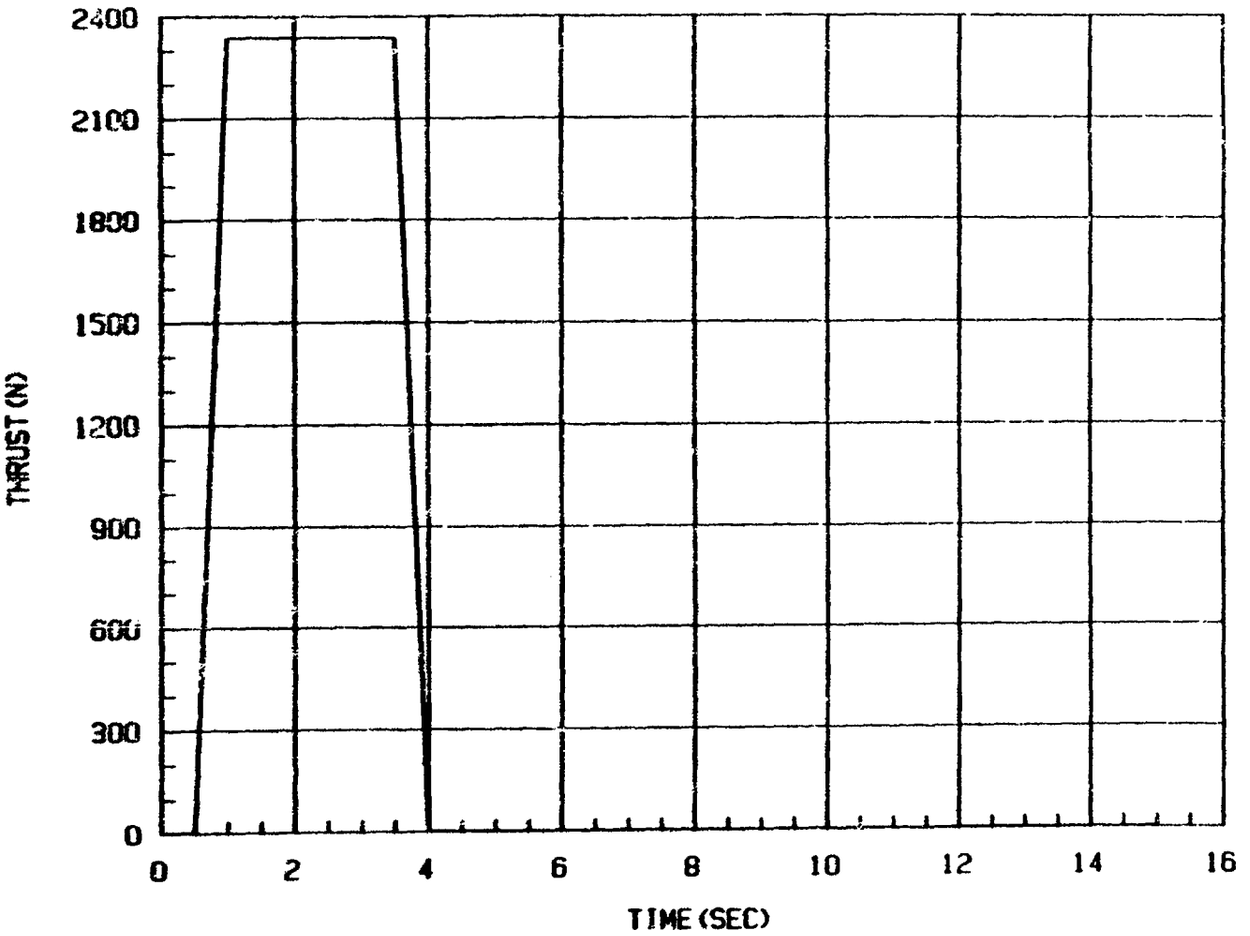

Figure 6.1. Rocket Motor Thrust Profile Model

This computational model incorporates a transfer function furnished by NWC to provide the vane temperature data for comparison with the simulation results [Reference 8]. The transfer function, derived from experimental test data, is given by

$$\frac{T_3}{\text{Thrust}} = \frac{8}{(1.233S + 1)(50.76S + 1)} \qquad (6.1)$$

It should be noted that in this equation the thrust is in newtons and the temperature in degrees Fahrenheit above ambient.

Simulation inputs and associated heat transfer parameters, for the case herein, are listed in Appendix A with the simulation results presented below.

B. VANE THERMAL RESPONSE

DSL simulation results predicting the vane thermal response to input data of Appendix A, is shown in Figure 6.2. The figure shows that the computed shaft temperature profile (node 3) is significantly higher than that obtained in the NWC tests.

The greatest uncertainties associated with the 3-NODE model result from the calculation of "best estimate" values for R_{F1} and R_{F2} and corresponding film coefficients. An additional uncertainty arises when attempting to adequately model the mount "heat sink"

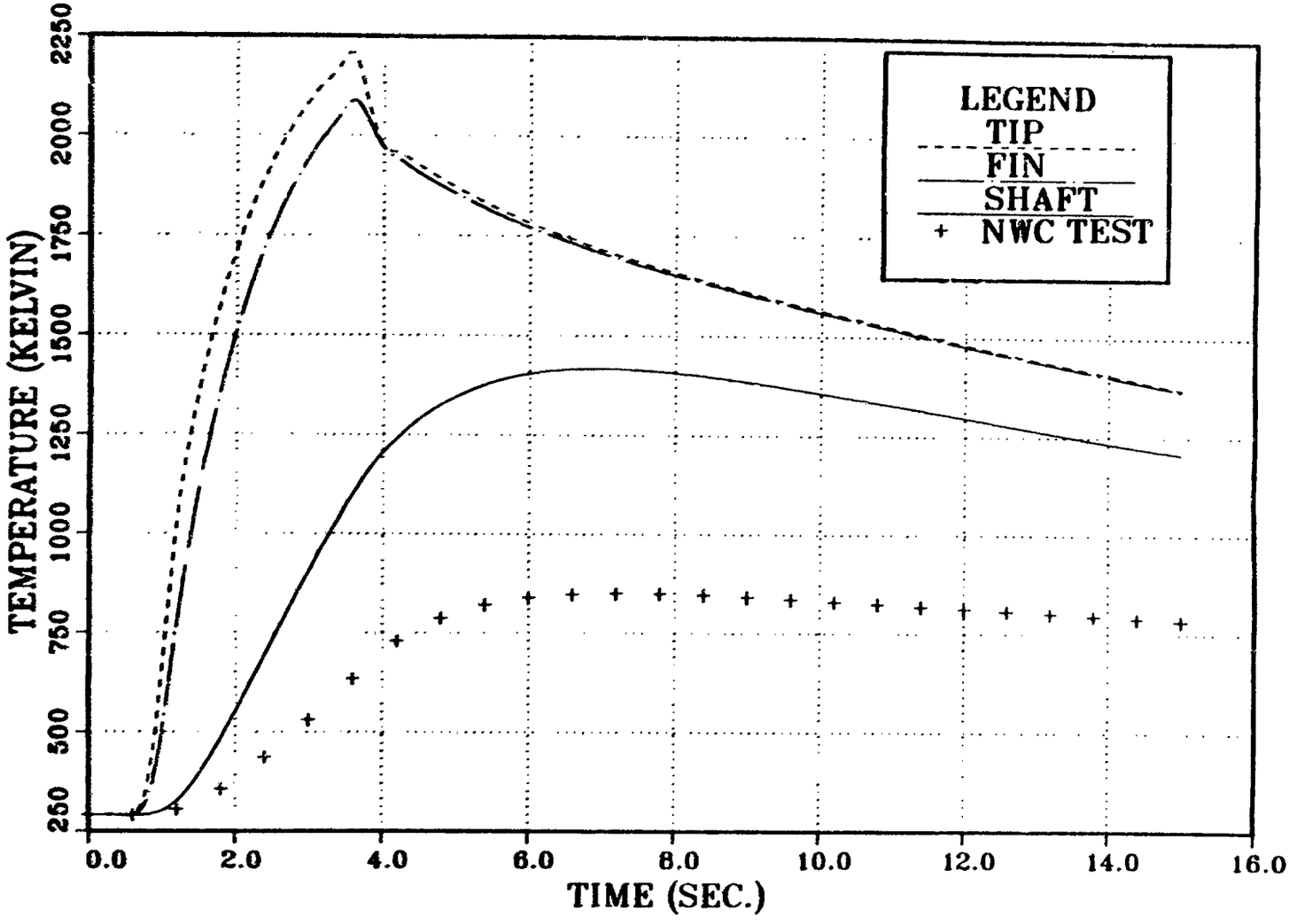

Figure 6.2. Vane Thermal Response

phenomena by a single mount resistance, R_{3G}. Preliminary experimentation with simulation, as detailed in reference 5, has led to the insight that the dominant factor affecting the maximum shaft temperature is the mount thermal resistance. The dynamic temperature rise of the shaft, however, is mainly controlled by the convective thermal resistance.

Figure 6.3 shows the sensitivity of the shaft temperature response to the adjustments of convective film coefficients. This figure clearly illustrates that in order to obtain reasonable agreement between simulation actual it will be necessary to lower these coefficients by a reduction factor (R_F) of approximately 70%. It has been postulated that this reduction factor may provide some insight into the relative magnitude of the cooling effects of radiation and ablation, which thusfar have been omitted from the analysis. It is equally apparent from this figure, that the model is capable of accurately reproducing the main transient characteristics of the vane thermal response.

C. SUMMARY

The 3-NODE model incorporating a mount thermal resistance of R_{3G} = 10.3 K/W and a reduction factor of R_F = 0.72 yields results of the sort shown in Figure 6.4. It is noteworthy that the results of the simulation indicate

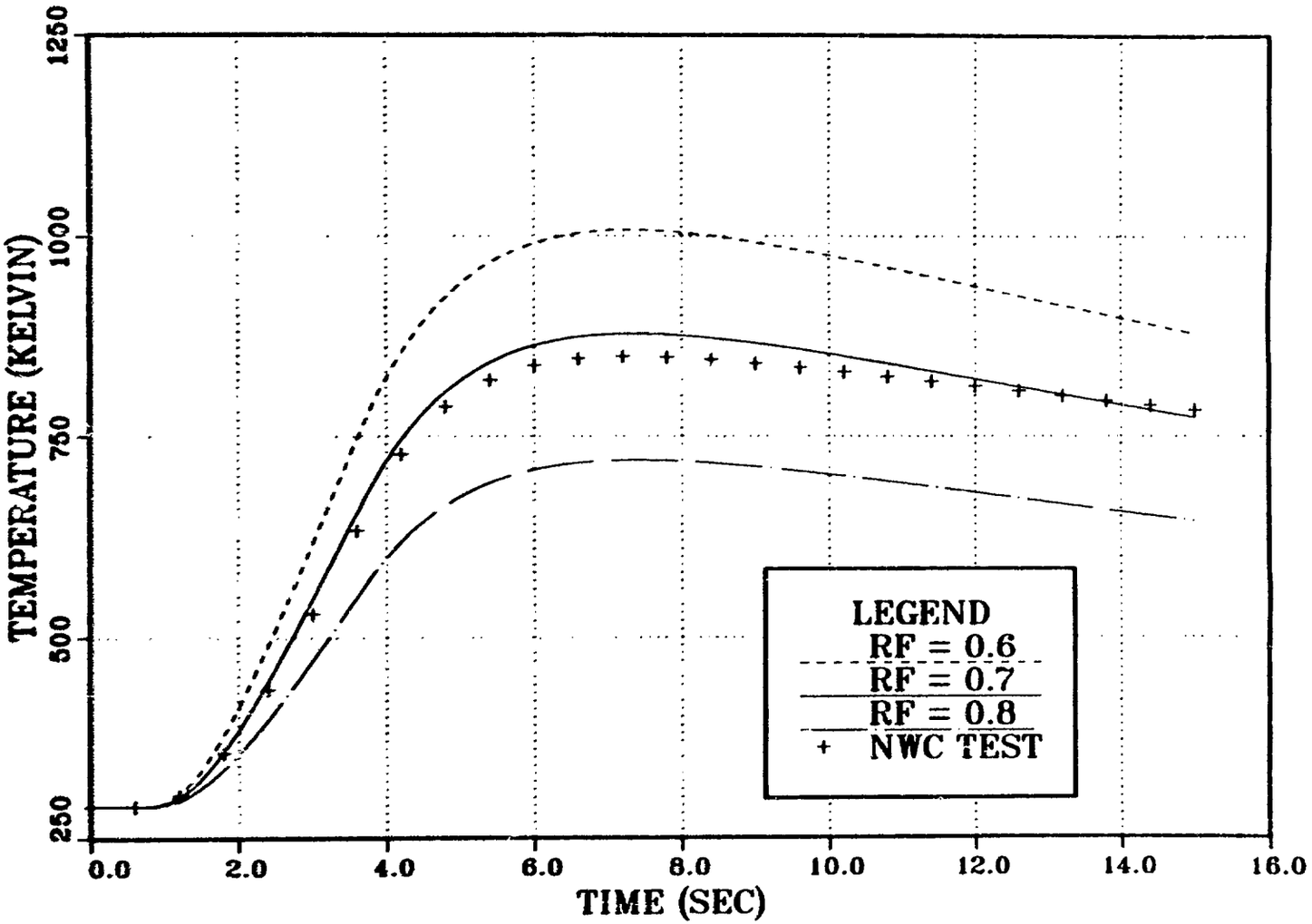

Figure 6.3. Shaft Temperature Profiles for Various Values of R_F

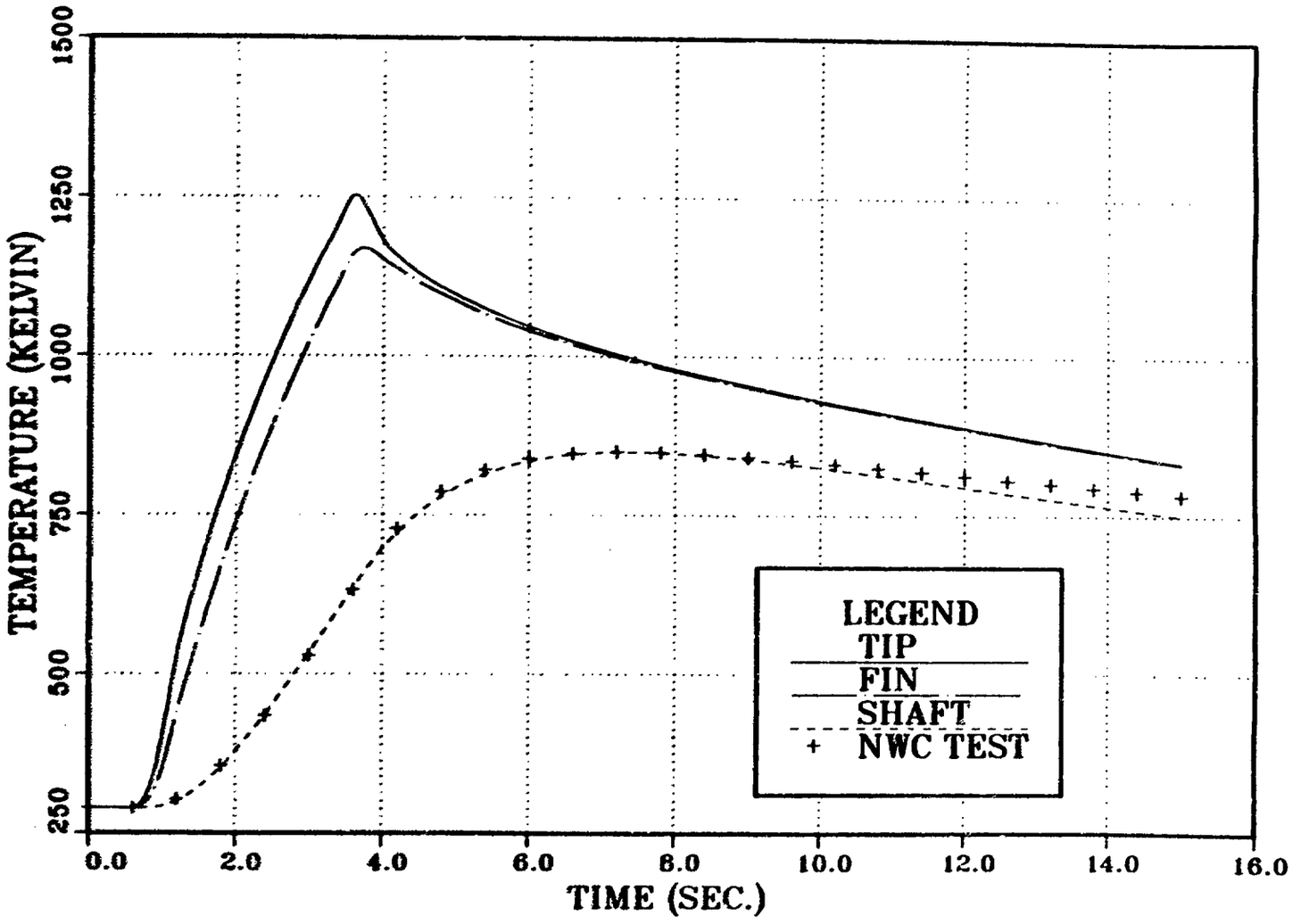

Figure 6.4. Vane Thermal Response with R_F=0.72

that it might be feasible to predict the bulk thermal behavior of specified critical elements of the jet vane, namely the tip, fin and shaft. Also important is the model simplicity, a prerequisite for system-identification analysis which is the subject of the next chapter.

VII. SIMPLE FOUR NODE MODEL

A. FOUR NODE CONFIGURATION

The goal of the work presented herein has been to extend the results reported in Reference 8 by utilizing additional experimental data available from NWC tests. These include subscale data from the thermal response of two thermocouples located in the shaft and mount regions.

To fully exploit this additional information it has been necessary to enhance the thermal model with an additional calculation node. Hence, the model illustrated in Figure 4.3 has been revised as shown in Figure 7.1.

Energy balance equations for this configuration are as follows:

$$sT_1 = \frac{-T_1}{C_1}\left[\frac{1}{R_{1i}} + \frac{1}{R_{F1}}\right] + \frac{T_{R1}}{C_1R_{F1}} + \frac{T_i}{C_1R_{1i}} \qquad (7.1)$$

$$sT_2 = \frac{-T_2}{C_2}\left[\frac{1}{R_{23}} + \frac{1}{R_{F2}} + \frac{1}{R_{i2}}\right] + \frac{T_{R2}}{C_2R_{F2}} + \frac{T_i}{C_2R_{i2}} + \frac{T_3}{C_2R_{23}} \qquad (7.2)$$

$$sT_3 = \frac{-T_3}{C_3}\left[\frac{1}{R_{34}} + \frac{1}{R_{23}}\right] + \frac{T_2}{C_3R_{23}} + \frac{T_4}{C_3R_{34}} \qquad (7.3)$$

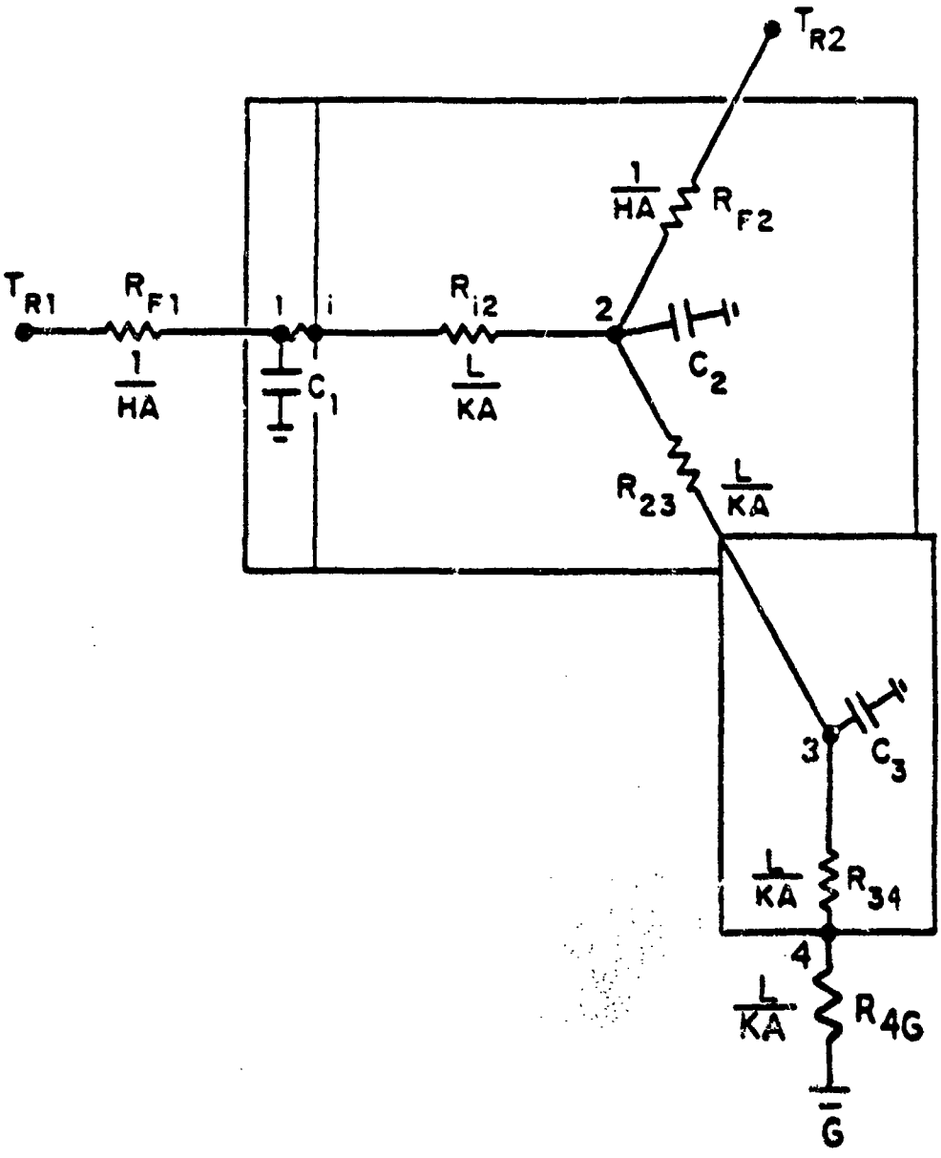

Figure 7.1 Simple Four Node Model Configuration

$$T_4 = T_3 \left[\frac{1}{R_{34}+R_{4G}} \right] + T_g \left[\frac{R_{34}}{R_{34}+R_{4G}} \right] \qquad (7.4)$$

The internal node designated (i) in Figure 7.1 is not a storage node and the energy balance for this node yields the following expression

$$\frac{T1 - Ti}{R1i} = \frac{Ti - T2}{Ri2} \qquad (7.5)$$

Using equation (7.5) to eliminate Ti from equations (7.1) and (7.2) gives the following set of four governing equations in state space from:

$$\dot{T}_1 = -T_1 \left[\frac{1}{R_{F1}} + \frac{1}{R_{12}} \right] + T_2 \left[\frac{1}{C_1 R_{12}} \right] + T_{R1} \left[\frac{1}{C_1 R_{F1}} \right] \qquad (7.6)$$

$$\dot{T}_1 = T_1 \left[\frac{1}{C_2 R_{12}} \right] - \frac{T_2}{C_2} \left[\frac{1}{R_{F2}} + \frac{1}{R_{12}} + \frac{1}{R_{23}} \right] + T_3 \left[\frac{1}{C_2 R_{23}} \right] + T_{R2} \left[\frac{1}{C_2 R_{F2}} \right] \qquad (7.7)$$

$$\dot{T}_3 = T_2 \left[\frac{1}{C_3 R_{23}} \right] - \frac{T_3}{C_3} \left[\frac{1}{R_{23}} + \frac{1}{R_{34}} \right] + T4 \left[\frac{1}{C_3 R_{34}} \right] \qquad (7.8)$$

$$T_4 = T_3 \left[\frac{R_{4G}}{R_{34} + R_{4G}} \right] + T_G \left[\frac{R_{34}}{R_{34} + R_{4G}} \right] \qquad (7.9)$$

where $R_{12} = R_{1i} + R_{i2}$.

B. THE "SYSTEM BUILD" MODEL

The system of equations defined above, have been modeled in the SYSTEM BUILD [Ref. 13] format of the personal computer version of the software package MATRIXx [Ref. 14]. The SYSTEM BUILD model is illustrated in Appendix B and the reader should note the hierachical nesting of the "super-blocks". A brief description of this arrangement will be given here.

To help illustrate this SYSTEM BUILD arrangement, it is useful to define the following parameters:

$$a_{11} = (a_{12} + a_{13} + b_{11}), \quad a_{12} = 1/C_1R_{12}$$

$$a_{21} = 1/C_2R_{12}, \quad a_{22} = (a_{21} + a_{23} + b_{22}), \quad a_{23} = 1/C_2R_{23}$$

$$a_{32} = 1/C_3R_{23}, \quad a_{33} = (a_{32} + a_{34}), \quad a_{34} = 1/C_3R_{34}$$

$$a_{43} = R_{4G}/(R_{34} + R_{4G})$$

$$b_{11} = 1/C_1R_{F1}, \quad b_{22} = 1/C_2R_{F2} \qquad (7.10)$$

With the above parameters thus defined, the state equations can be simplified as follows

$$\dot{T}_1 = -a_{11}T_1 + a_{12}T_2 + b_{11}T_{R1} \qquad (7.11)$$

$$\dot{T}_2 = a_{21}T_1 - a_{22}T_2 + a_{23}T_3 + b_{22}T_{R2} \qquad (7.12)$$

$$\dot{T}_3 = a_{32}T_2 - a_{33}T_3 + a_{34}T_4 \qquad (7.13)$$

In this study, all temperatures have been referred to ambient temperature (T_G), hence equation 7.9 can be written as

$$T_4 = a_{43}T_3 \qquad (7.14)$$

In this study, the SYSTEM BUILD thermal model is comprised of eight super-blocks:

NOD1IN, NOD2IN, NOD3IN

NODE1, NODE2, NODE 3, NODE4

VANE

The input to the model is the ramp-up, plateau, ramp-down profile previously described in Chapter VI. This input with a maximum plateau level of unity is supplied to both NOD1IN and NOD2IN, whereas NOD3IN does not require the time-varying input. These first three blocks compute the coefficients necessary for the state equations modeled by the next three blocks. Super-block NODE4 requires only one input from NODE3. In NOD1IN, for example, the input is multiplied by b_{11} and T_{R1}. Also in NOD1IN the parameter a_{12} is generated by means of a step function and is summed with b_{11} to form a_{11}. Thus the outputs of NOD1IN are a_{11}, a_{12} and $b_{22}T_{R1}$ and a_{32}, a_{33}, a_{34} respectively.

As illustrated in Appendix B, the first three super-blocks listed above are nested within the next three blocks respectively and NODE4 requires no nested block. In NODE1, for example, the outputs of NOD1IN are combined with the external input T_2 to form the state equation

$$\dot{T}_1 = -a_{11}T_1 + a_{12}T_2 + b_{11}T_{R1} \qquad (7.15)$$

An integrator is then used to convert $\dot{T}_1$ to T_1, which is the NODE1 output. Again, NODE2, NODE3 and NODE4 are

similar in function and provide outputs T2, T3 and T4. The superblock VANE connects all four of these blocks together and provides the simultaneous solution for the four nodal temperatures.

C. SIMULATION RESULTS/SYSTEM IDENTIFICATION

The first step in the execution of the SYSTEM BUILD model is to check the model by means of the ANALYZE command [Ref. 13]. Next, one of six integration algorithms may be selected. The results presented herein have been obtained with the variable Kutta-Merson method which is an explicit, fourth order, one-step method. This method employs the largest time step possible while remaining within error tolerances. The maximum step size is equal to the time increment specified for the simulation. The final step is executing the SIM command, as in "Y = SIM (T, U)", where T is the time vector and U is the input, both of which must be provided. For the results described here, T is a 151 x 1 vector created by dividing 15 seconds into 0.1 second increments. U is the 151 x 2 matrix depicting the two ramp-up, unity plateau, ramp down profiles previously described.

1. NWC Transfer Function Results

Figure 7.2 shows the results of simulation using the SYSTEM BUILD model to predict the vane thermal response incorporating "best estimate" values of R_{34} = 3.0 K/W

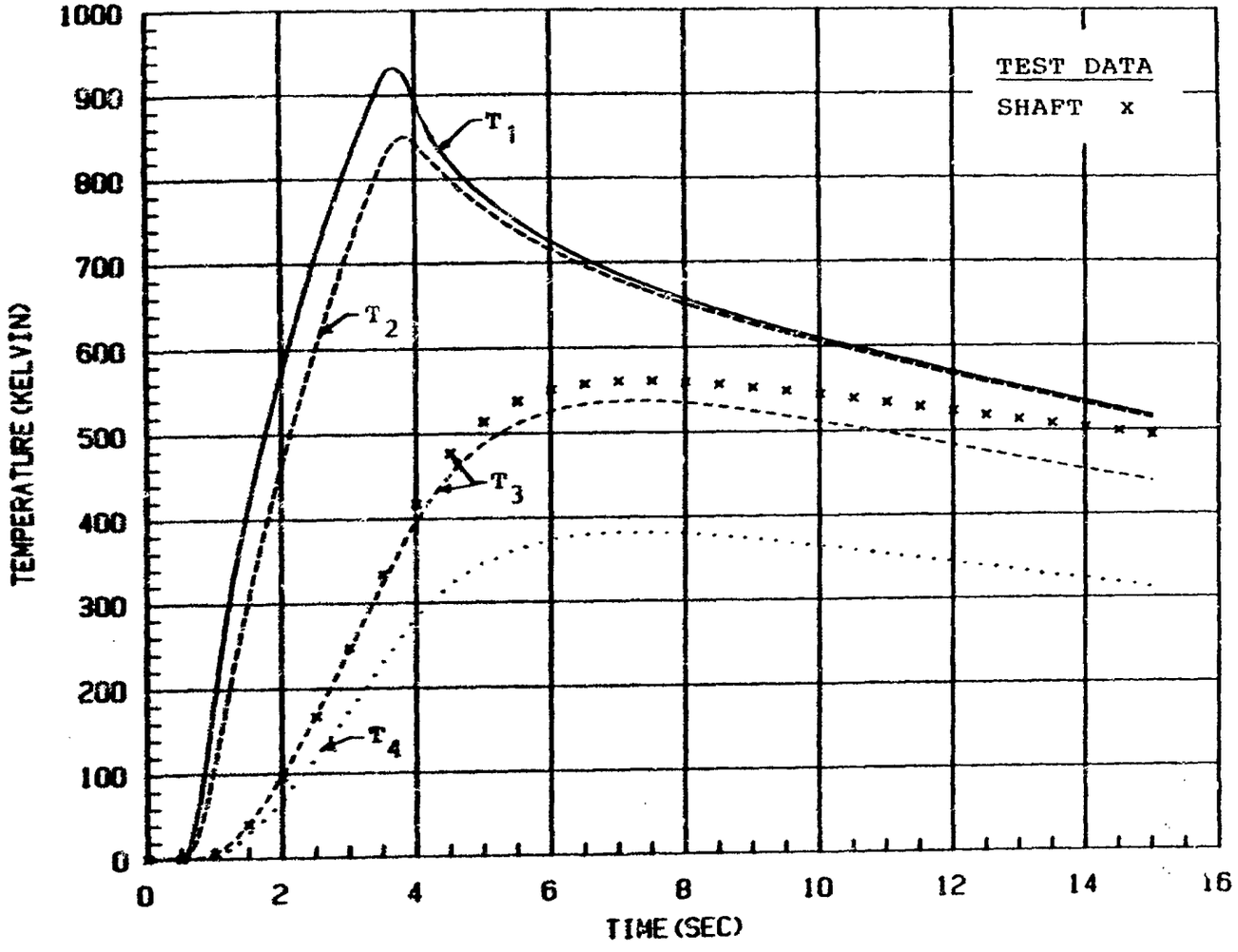

Figure 7.2. Comparison of Simulation and NWC Transfer Function Results

(a_{34}=.33) and R_{4G} = 7.3 K/W (a_{43}=.709). Data from the NWC transfer function described in Chapter VI has been used for comparison.

The model was set up for system identification, using the MAXLIKE function [Ref. 8, 15]. Figure 7.3 shows the results for shaft temperature after having reduced a_{34} and a_{43} to the MAXLIKE specified values of .1633 and .550 respectively. These results are clearly excellent and give encouragement that the Parametric System Identification (PSI) capability of the MAXLIKE command function is a feasible design tool.

2. NWC 1/4-Scale Test Firings

Event (2) and event (6) are names given to separate 1/4-scale VLMB rocket motor test firings conducted by NWC. The only planned difference in the two tests was the type of propellant burned with event (2) using non-aluminized HTPB (Hydroxyl-Terminated Polybutadien) and event (6) burning 18% Aluminized HTPB. In both tests, two thermocouples were attached to each vane in the shaft and mount regions. The thermal response of these thermocouples were recorded and the results are included in Appendix C along with the rocket motor ballistics data and propellant properties. It should be noted, however, that the shaft thermocouples failed 1.4 seconds into event (6) test firing. Hence no usable shaft temperature data from event (6) is available for comparison purposes. Event (2) stagnation temperature T_0=2650K and

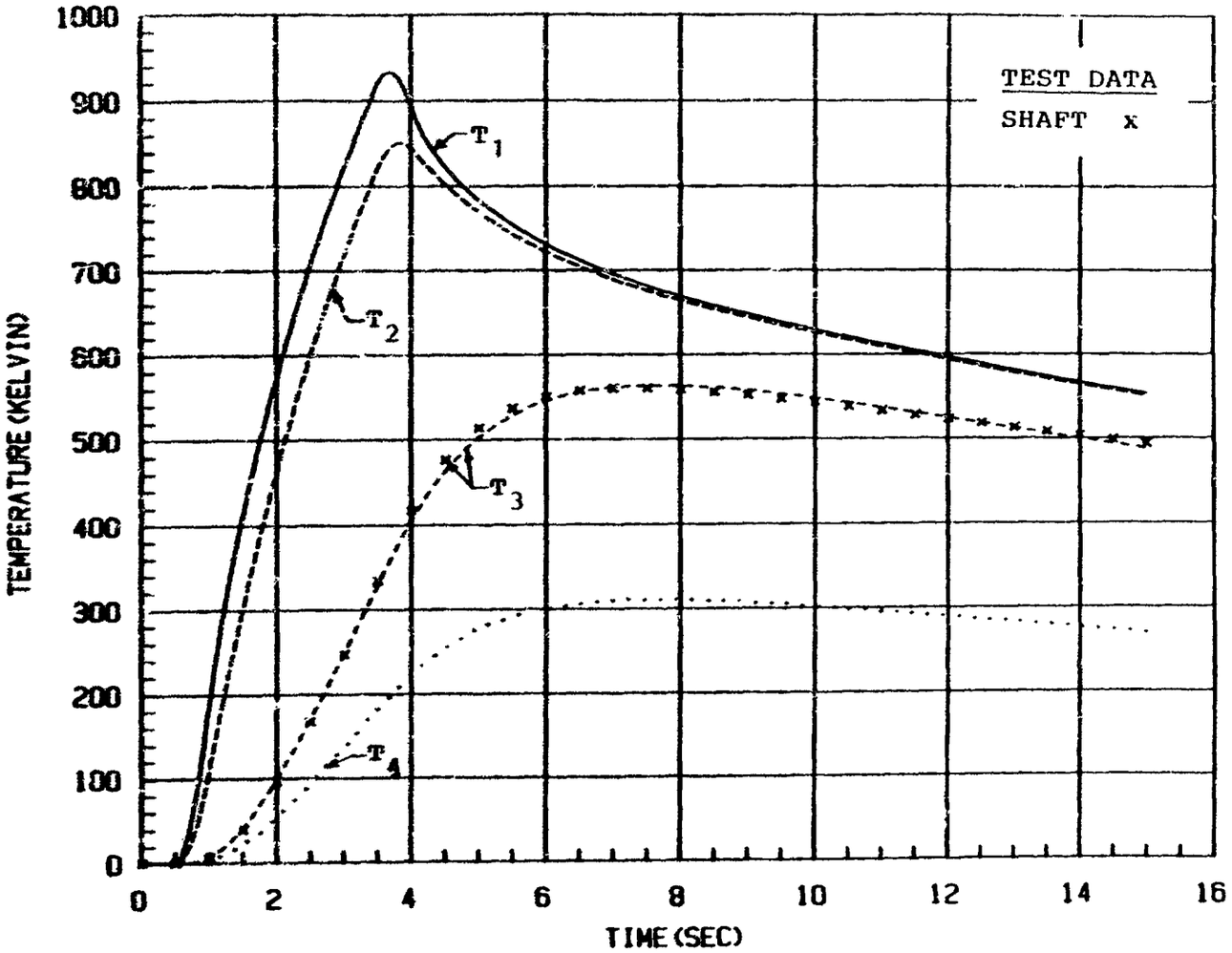

Figure 7.3. Comparison of Simulation and NWC Transfer Function Results After PSI

ambient temperature of 290K yield T_{R1}=2360K and T_{R2}=2260K. Event (5) stagnation temperature T_0=3275K and ambient temperature of 305K yield T_{R1}=2970K and T_{R2}=2870K.
It should be noted that the mount hardware of event (6) and event (2) each use different type fasteners.

3. Event (2) Simulation Results

Figure 7.4 is the result of a Parametric Simulation Identification (PSI) execution using initial parameter values of a_{34} = .1633 and a_{43} = .5500 taken from the previous results of figure 7.3. The MAXLIKE values obtained are a_{34} = .17 and a_{43} = 0.56 as the result of comparing model and experimental shaft temperatures. Although figure 7.3 indicates excellent agreement between predicted and actual shaft temperatures, the time constant of NODE 4, as modelled, is significantly less than that observed in actual test firings.

4. Event (6) Simulation Result

Figure 7.5 is the result simulating the vane thermal response at the elevated input temperatures of T_{R1} = 2970K and T_{R2} = 2870K with parameters a_{34} and a_{43} remaining at the previous values of 0.17 and 0.56 respectively. This figure clearly indicates the disparity between the model NODE 4 and actual mount time constants. Figure 7.6 is the result of increasing R_{4G} in equation (7.9) to a value of 9.9 K/W to more closely approximate the actual mount temperature at time = 15s.

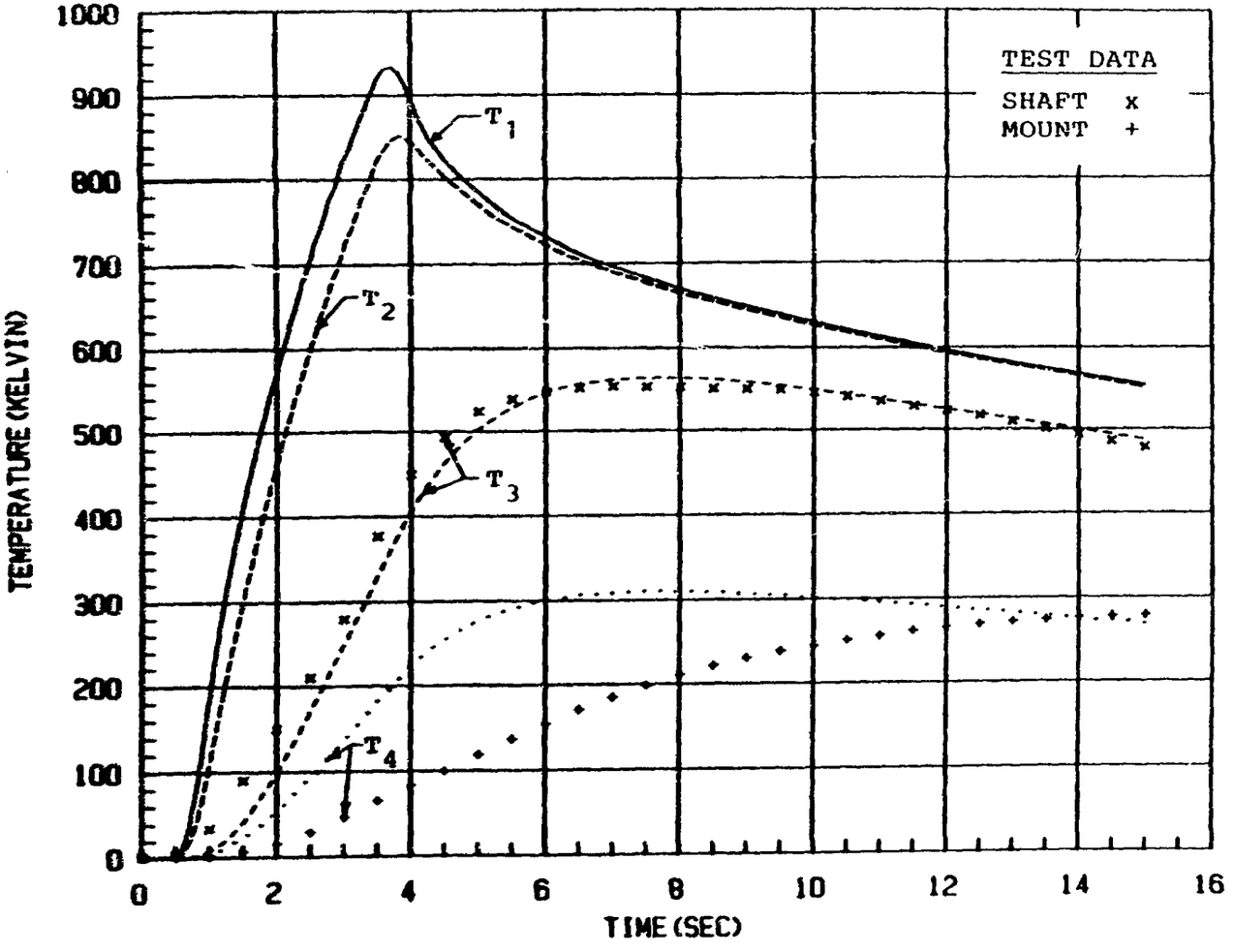

Figure 7.4. Comparison of Simulation and Event (2) Results

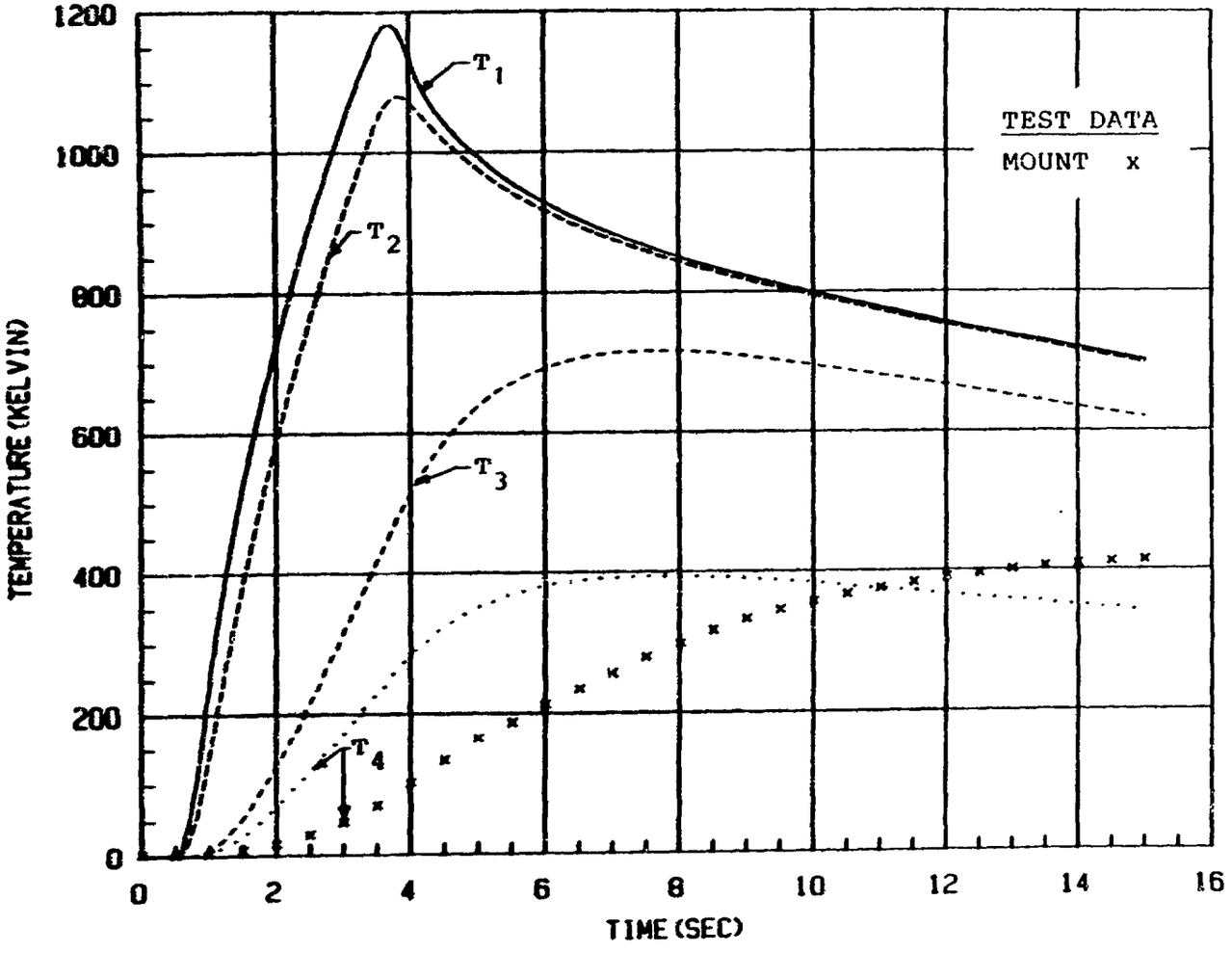

Figure 7.5. Comparison of Simulation and Event (6) Results, R_G=7.2 K/W

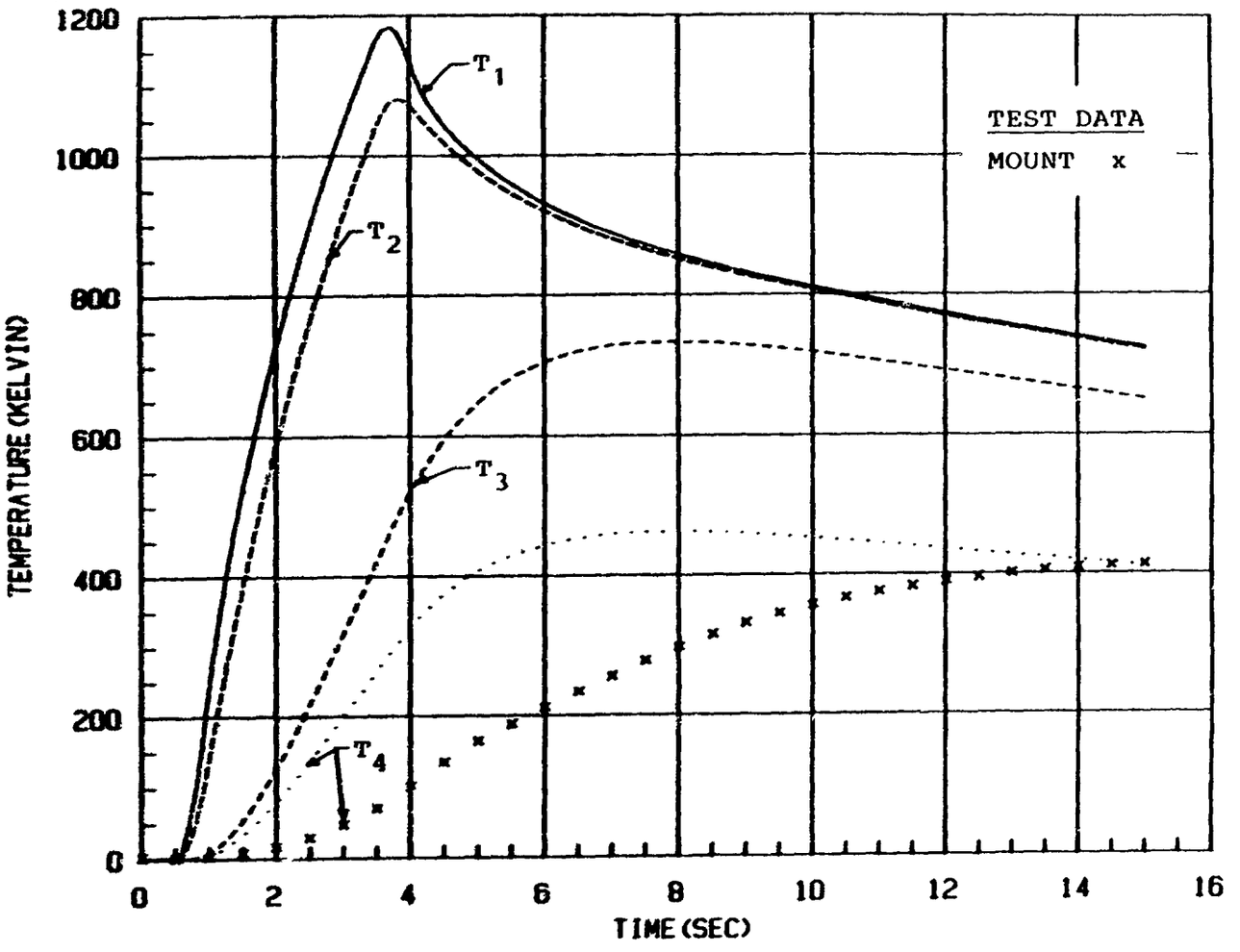

Figure 7.6. Comparison of Simulation and Event (6) Results, R_G=9.8 K/W

From the results of Figures 7.4 and 7.5 it became apparent that the simple conduction path linking nodes 3 and 4 is an inadequate representation of the vane/mount response. It is obvious that the T_4 node responds with a time constant significantly different than that of the T_3 node. Correction of this modeling discrepancy is the subject of the next chapter.

VIII. REVISED FOUR-NODE MODEL

A. REVISED FOUR NODE CONFIGURATION

In order to vary the time constant at node 4 it was necessary to enhance the simple four node model with an additional capacitance C_4 located at this node. Thus, the model illustrated in Figure 7.1 has been revised as shown in Figure 8.1.

Energy balance equations for this configuration remain unchanged from those previously described except for node 4, which is given by

$$\dot{T}_4 = T_3 \left[\frac{1}{C_4 R_{34}}\right] - T_4 \left[\frac{1}{C_4 R_{34}} + \frac{1}{C_4 R_{4G}}\right] \qquad (8.1)$$

The above expression can be simplified as follows

$$\dot{T}_4 = a_{43} T_3 - a_{44} T_4 \qquad (8.2)$$

where

$$a_{43} = 1/C_4 R_{34},\ a_{4G} = 1/C_4 R_{4G},\ a_{44} = a_{43} + a_{4g} \qquad (8.3)$$

B. REVISED "SYSTEM BUILD" MODEL

The revised SYSTEM BUILD thermal model is comprised of nine super-blocks.

NOD1IN, NOD2IN, NOD3IN, NOD4IN

NODE1, NODE2, NODE3, NODE4G

VANE7

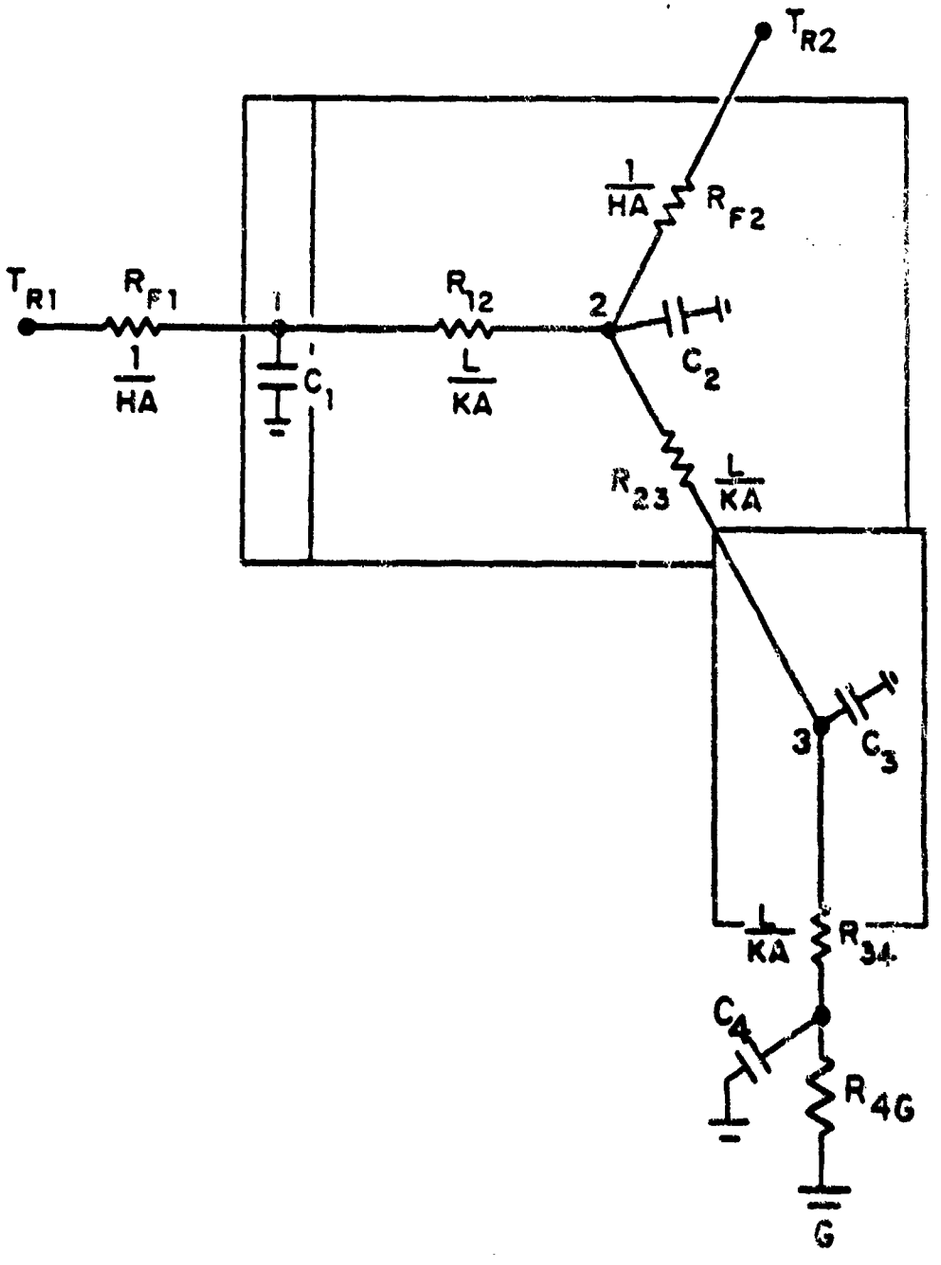

Figure 8.1 Revised Four-Node Model Configuration

this model arrangement is identical to the initial configuration illustrated in Appendix B except for the addition of block NOD4IN shown in Figure 8.2 and the replacement block NODE4 with block NODE4G illustrated in Figure 8.3. The input to NOD4IN is the external input T_3 from NODE3. In NOD4IN the parameters a_{43} and a_{4G} are generated by a step function. Parameter a_{43} is multiplied by the input T_3 to form $a_{43}T_3$ and summed with a_{4G} to form a_{44}. In NODE4G the outputs of NOD4IN are combined with the internal input T_4 to form $\dot{T}_4$. An integrator is then used to convert $\dot{T}_4$ to T_4, which is the NODE4G output. Super-block VANE7 connects the four NODE super-blocks together as illustrated in Figure 8.4 and provides the simultaneous solution for the four nodal temperatures.

C. SIMULATION RESULTS/SYSTEM IDENTIFICATION

1. Event (2) Results

Figure 8.5 is the result of simulation using initial values of R_{34} = 5.9K/W, R_{4G} = 7.2 K/W and C_4 = 1.0 J/K, which in turn yield parameter values a_{34} = .17, a_{43} = .17 and a_{44} = .14. This figure shows excellent agreement between the model and actual mount thermal responses.

Figure 8.6 is the result of a three-step PSI execution using initial parameter values of a_{34} = 0.17, a_{43} = 0.17 and a_{44} = 0.14. In the first step only

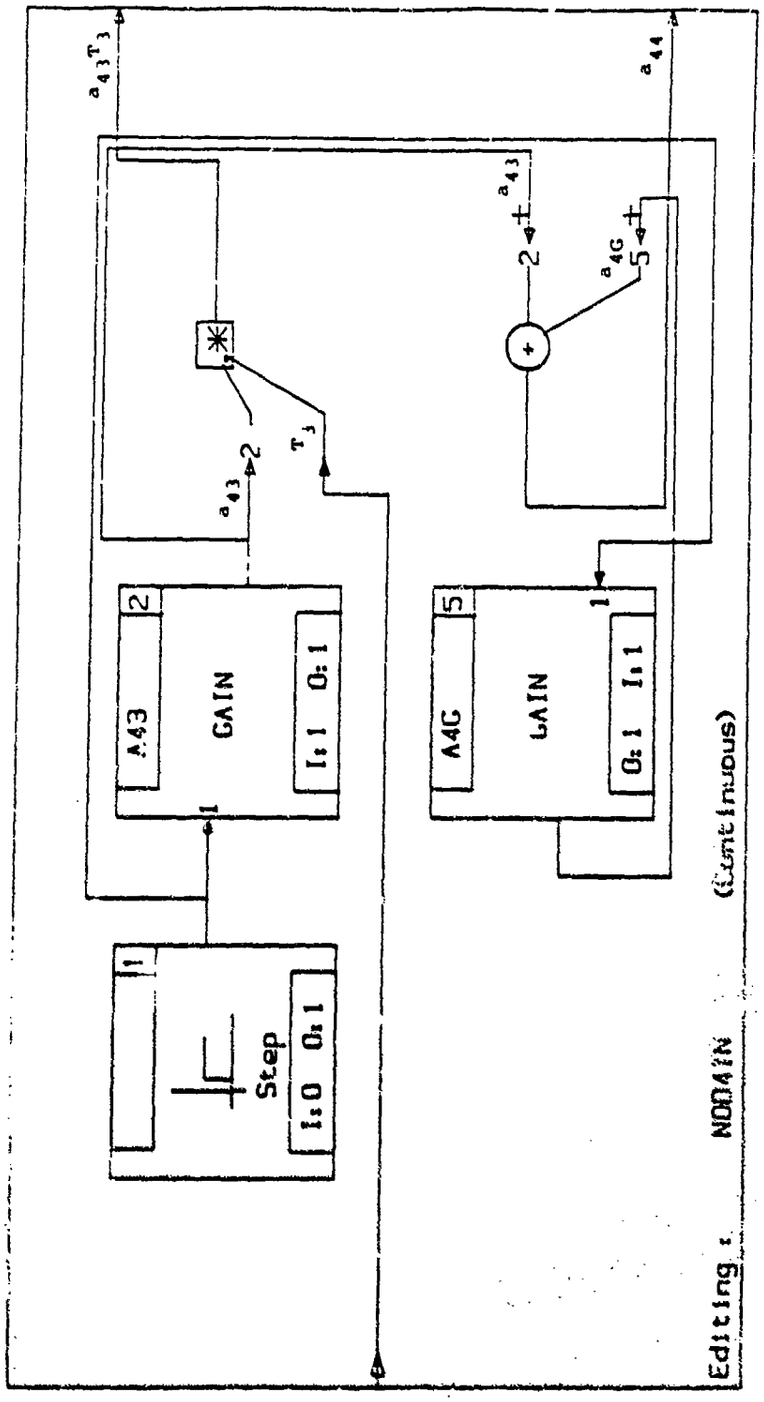

Figure 8.2. SYSTEM BUILD Super-Block NOD4IN

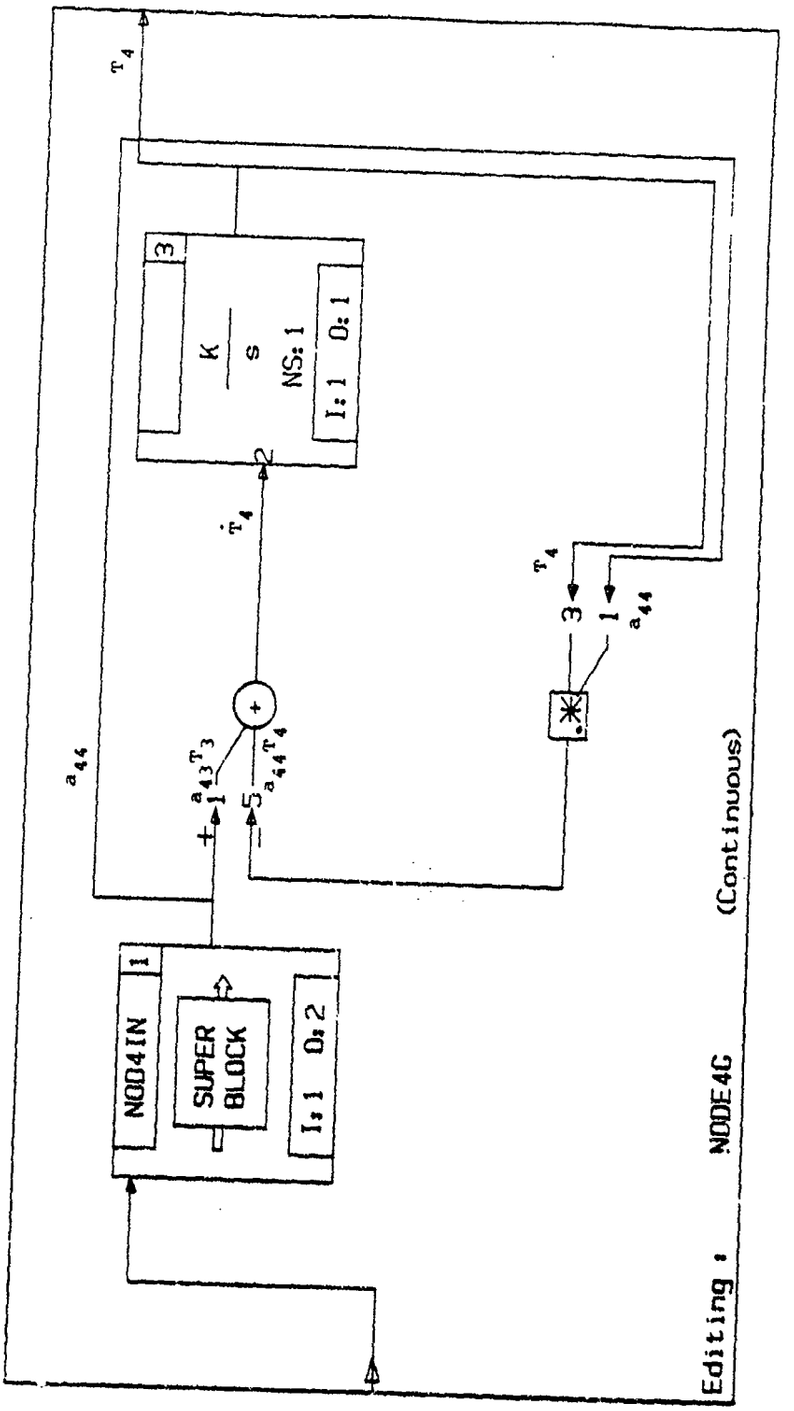

Figure 8.3. SYSTEM BUILD Super-Block NODE4G

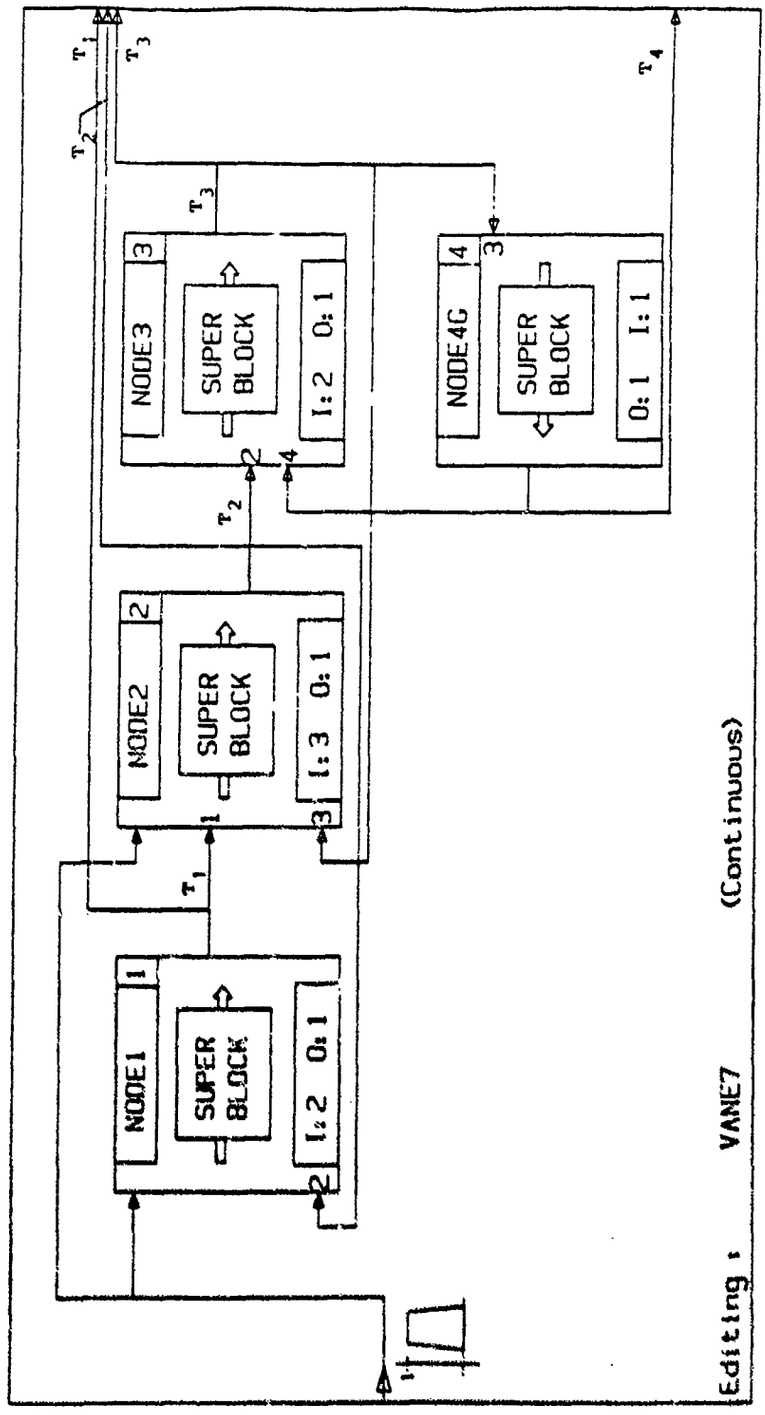

Figure 8.4. SYSTEM BUILD Super-Block VANE7

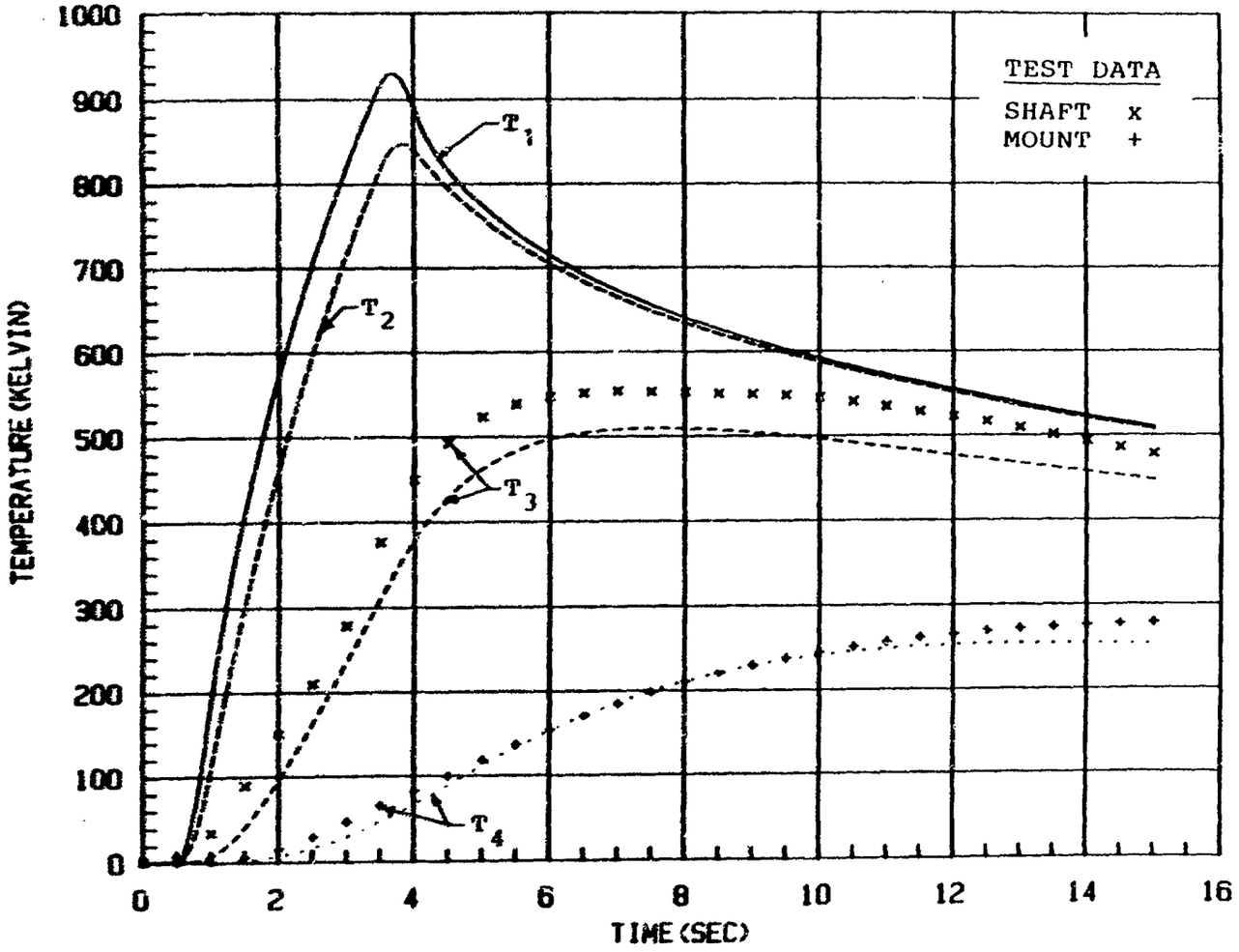

Figure 8.5. Comparison of Simulation and Event (2) Results

parameter a_{34} is varied in a PSI run of three iterations. The MAXLIKE value obtained based on T_3 is $a_{34} = 0.12$. In the next step, both parameters a_{43} and a_{4G} are allowed to vary in the PSI execution on both nodal temperatures T_3 and T_4. Although the MAXLIKE function is capable of operation on multiple outputs, this PSI effort failed due to inadequate computer memory storage. As an alternative approach, again with a_{43} and a_{4G} as the variable parameters, a PSI run was conducted based on T_4 alone and the MAXLIKE values obtained are $a_{43} = 0.17$ and $a_{4G} = 0.14$. These values give the excellent results shown in Figure 8.6.

3. Event (6) Results

Figure 8.7 is the result simulating vane thermal response at the elevated input temperatures of T_{R1} = 2970K and T_{R2} = 2870K with parameters a_{34}, a_{43} and a_{4G} remaining constant at the values identified in the previous PSI analysis.

Figure 8.8 is the result of a PSI execution using initial parameter values of $a_{43} = 0.17$ and $a_{4G} = 0.14$ taken from the previous results of Figure 8.6. The MAXLIKE values obtained are $a_{43} = 0.1693$ and $a_{4G} = 0.101$.

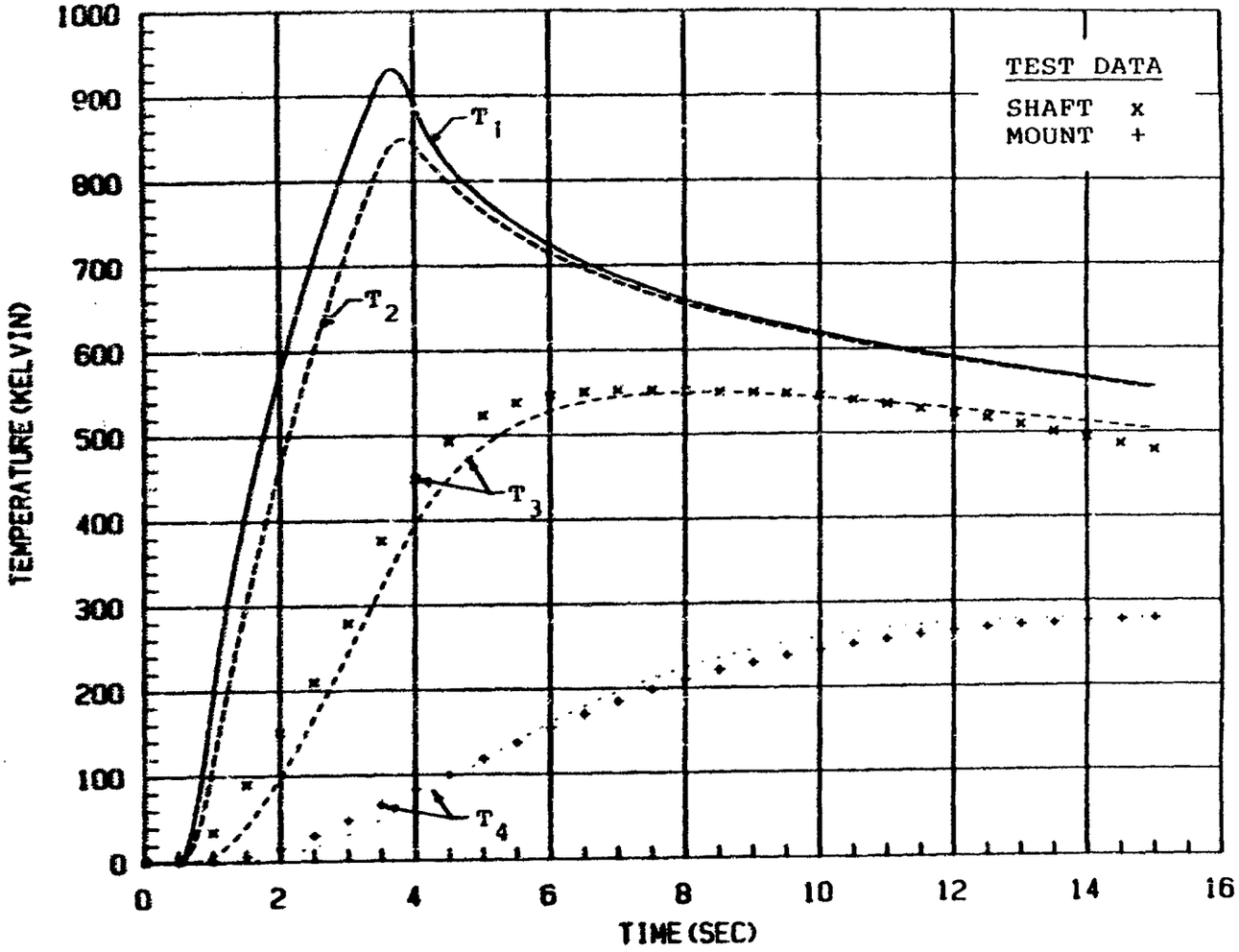

Figure 8.6. Comparison of Simulation and Event (2) Results After PSI

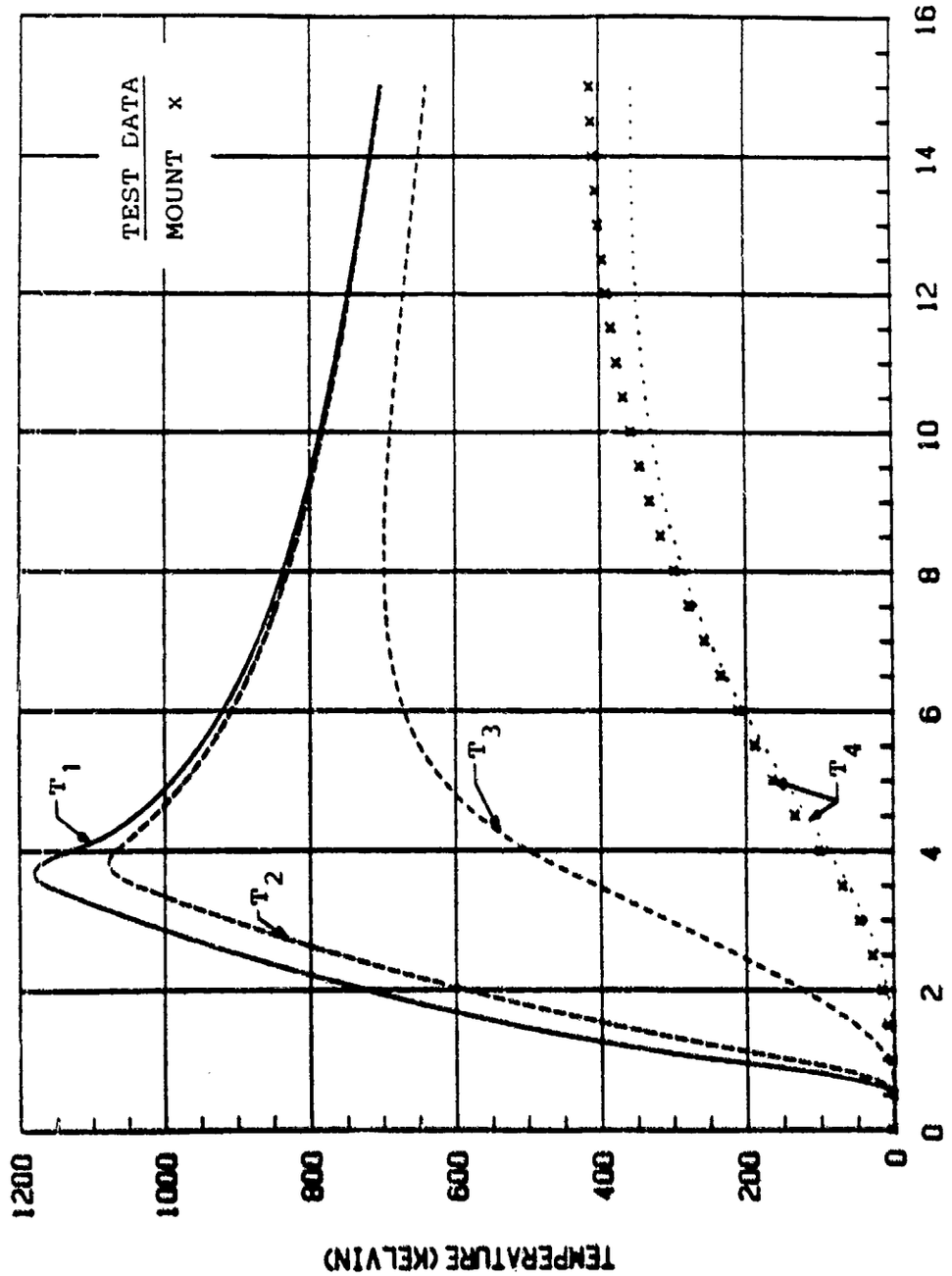

Figure 8.7. Comparison of Simulation and Event (6) Results

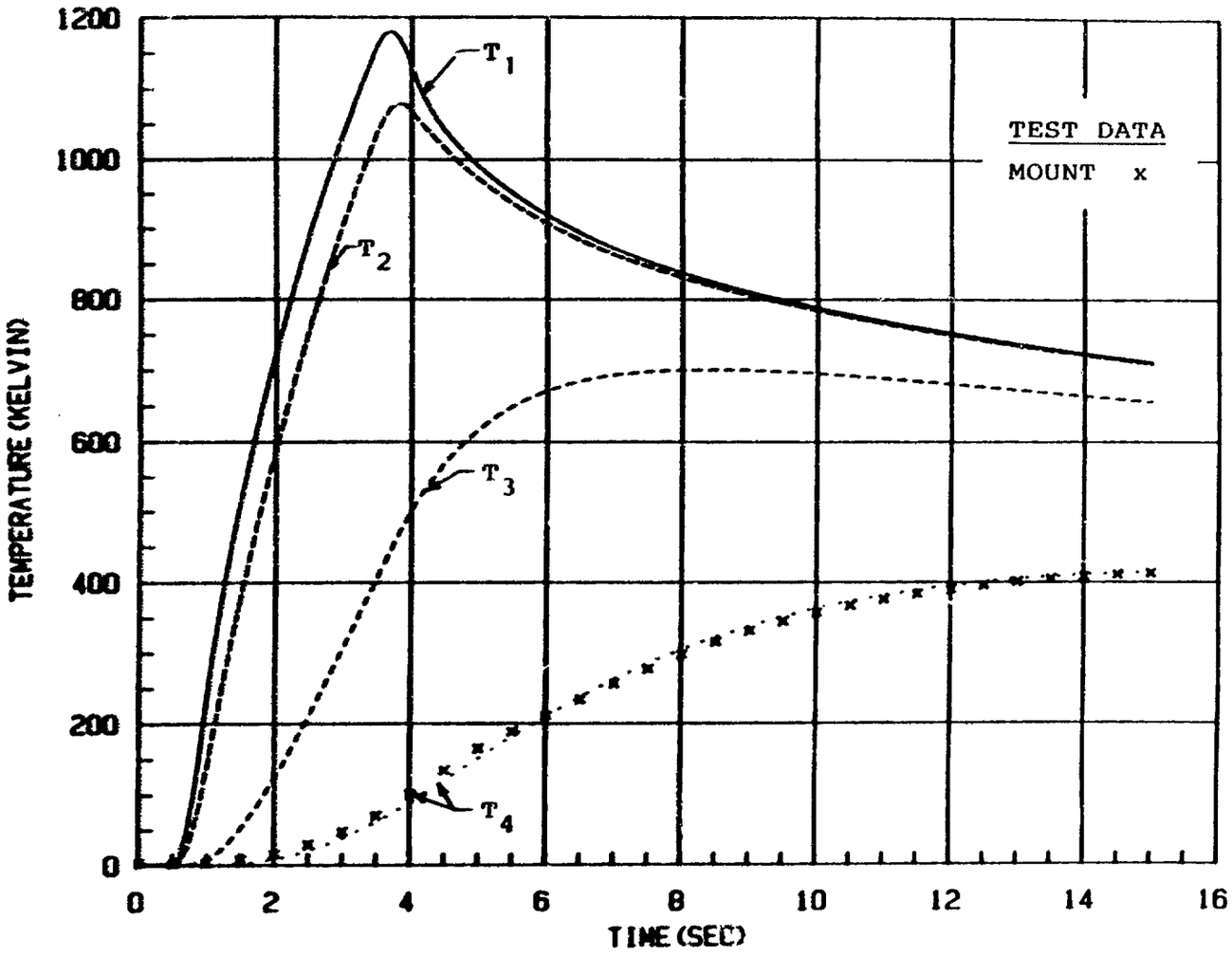

Figure 8.8. Comparison of Simulation and Event (6) Results After PSI

The node 4 time constant, resulting from addition of capacitance C_4 provides a good representation of mount thermal response, as indicated in the results outlined above. These results are further discussed in detail in the next chapter.

IX. CONCLUSIONS AND RECOMMENDATIONS

A. SUMMARY OF RESULTS

From the results presented in chapter VIII, it is quite apparent that the revised four-node model illustrated in Figure 8.1 provides an adequate representation of the vane/mount thermal interface.

The values of parameters a_{34}=0.12 and a_{43}=0.17 obtained from parametric system identification analysis using event (2) test data are identical to the values resulting from PSI execution of event (6) test data. These results are consistent with the fact that the jet vane employed in event (2) was identical to the vane used in event (6). Similarly, the differences in MAXLIKE resultant values a_{4G}=0.14 and a_{4G}=0.10 for events (2) and (6) respectively are an indication of actual variations in the mount hardware assemblies previously mentioned in Chapter VII. These results yield thermal model values of capacitance C_4=0.71 J/K and resistance R_{34}=8.3 K/W with R_{4G}=10.1 K/W for the event(2) mount and R_{4G}=13.9 K/W for the mount arrangement used in event (6).

B. CONCLUSIONS

The goal of the Modeling and Simulation study reported here has been to develop a dynamic thermal model of jet vane TVC devices and investigate the feasibility of using system identification methods to develop tools for use in the design of such vanes.

The SYSTEM BUILD capability of MATRIXx has been proven to be an excellent computational tool that provides both "state-of-the-art" graphical model building and simulation. This capability replaces the tedious DSL computer language programming employed in previous modeling and simulation development. SYSTEM BUILD, used in conjunction with MATRIXx interpreter, allows the designer to concentrate his or her efforts on design, analysis and simulation in an efficient graphical environment.

The development of MATRIXx as a design tool is further manifested by its system identification capabilities, in particular the MAXLIKE function used in the work reported here. In this study, the power of parametric system identification has been exploited in removing the some of the uncertainties associated with the revised four-node model.

The results presented in this thesis yield a measure of confidence that the thermal behavior of the jet vane TVC device can be modeled using a relatively simple "lumped-capacitance" type model configuration.

C. RECOMMENDATIONS

Further simulation and PSI analysis should be performed using a computer system such as a VAX-2000 work station and thereby ensuring adequate storage capacity is available to fully exploit the multi-input/multi-output systems capability of the MAXLIKE algorithm.

Also, a FORTRAN compiler should be incorporated into whatever system MATRIXx is loaded, in order to enhance the versatility of inputting test data. Data generated by other programs, or obtained from experiments must be converted to or stored in a form which can be read by the MATRIXx LOAD command. MATSAV is a FORTRAN subroutine designed to save external data in a proper format.

A logical next step in this study would be to adjust the parameters of the present model to full-scale values using direct scaling procedures such as those given in Chapter V. A comparison between the simulated thermal response of the model and recently acquired full-scale test data could be made and additional PSI conducted if necessary.

APPENDIX A

PRELIMINARY DSL SIMULATION PARAMETERS

ROCKET MOTOR

C_d = Nozzle Discharge Coefficient = .934

Γ = 0.65

C* = Characteristic Velocity = 1512 m/s

R_g = Gas Constant = 318.5 m^2/s^2 - K

K = Ratio of Specific Heats = 1.21

T_o = Stagnation Temperature = 2650K

$P_{0\infty}$ = Maximum Chamber Pressure = 15.76MPa

$P_{0\infty}/P_\infty$ = Nozzle Pressure Ration = 186

M_∞ = Mach Number at Nozzle Exit = 3.75

Maximum= 2325N

STAGNATION POINT

Staton Number = 8.53×10^{-3}

Nusselt Number = 43.1

Film Coefficient = 6.46×10^3 W/M^2 - K

Thermal Resistance = 5.69 K/W

TURBULENT BOUNDARY LAYER

Stanton Number = 3.01×10^{-3}

Nusselt Number = 438

Film Coefficient = 2.25×10^3 W/M^2 - K

Thermal Resistance = 0.634 K/W

APPENDIX B

SYSTEM BUILD BLOCK DIAGRAMS

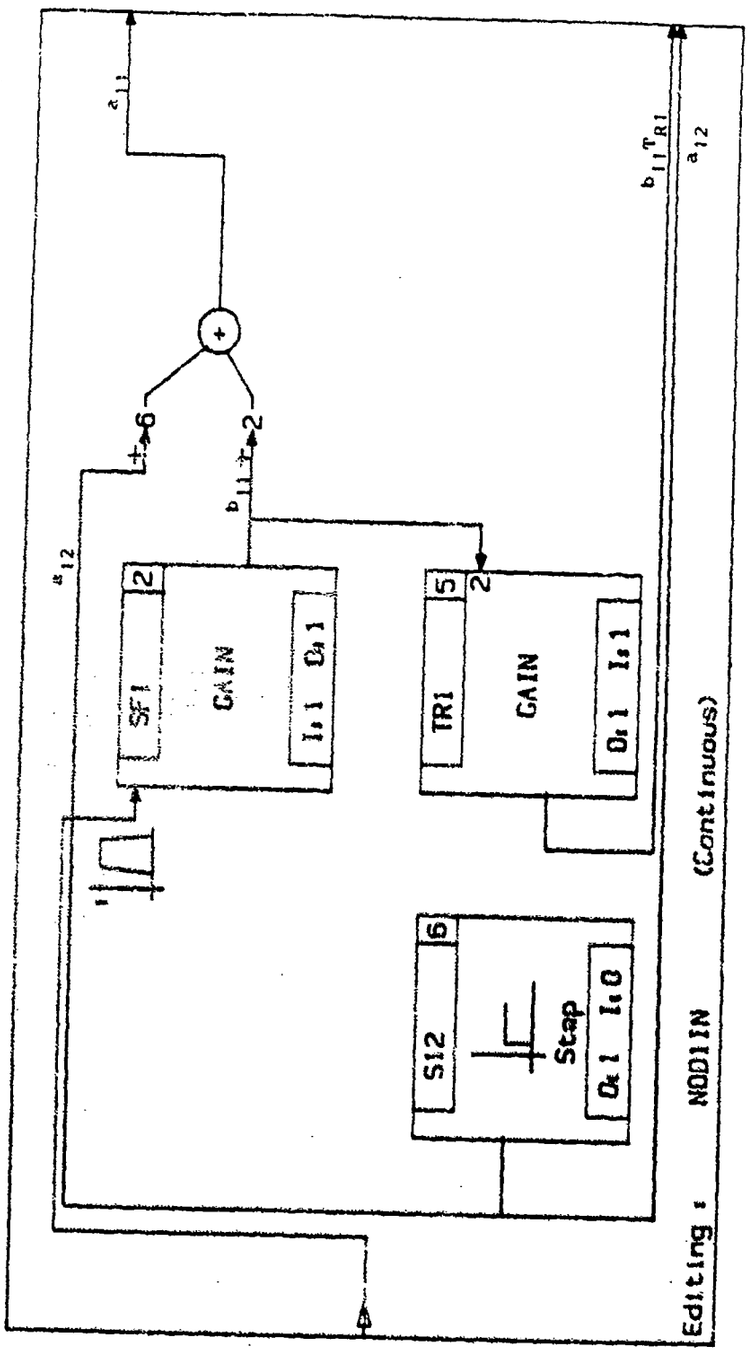

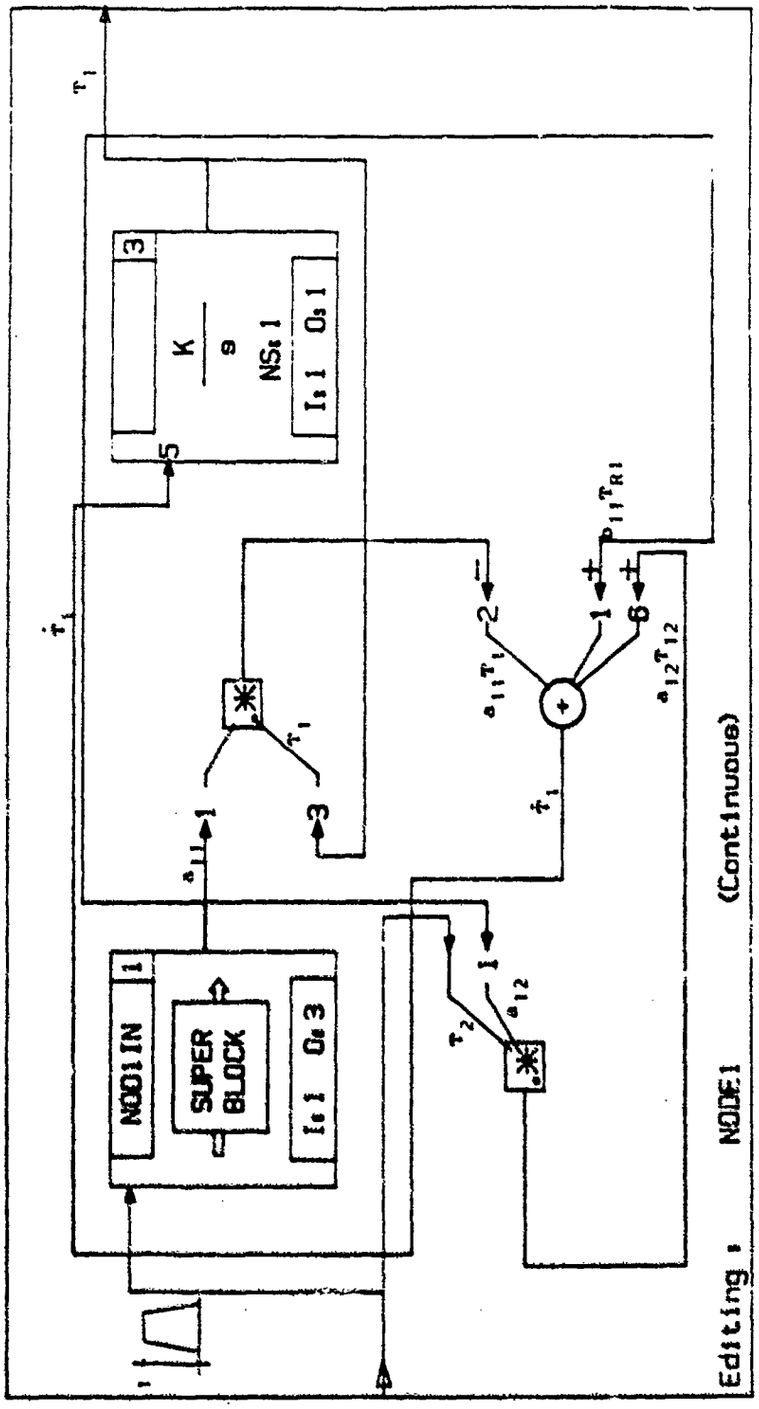
Editing : NODE1 (Continuous)
NODE1N
SUPER BLOCK
I: 1 O: 3
I: 1 O: 1
NS: 1
K
s

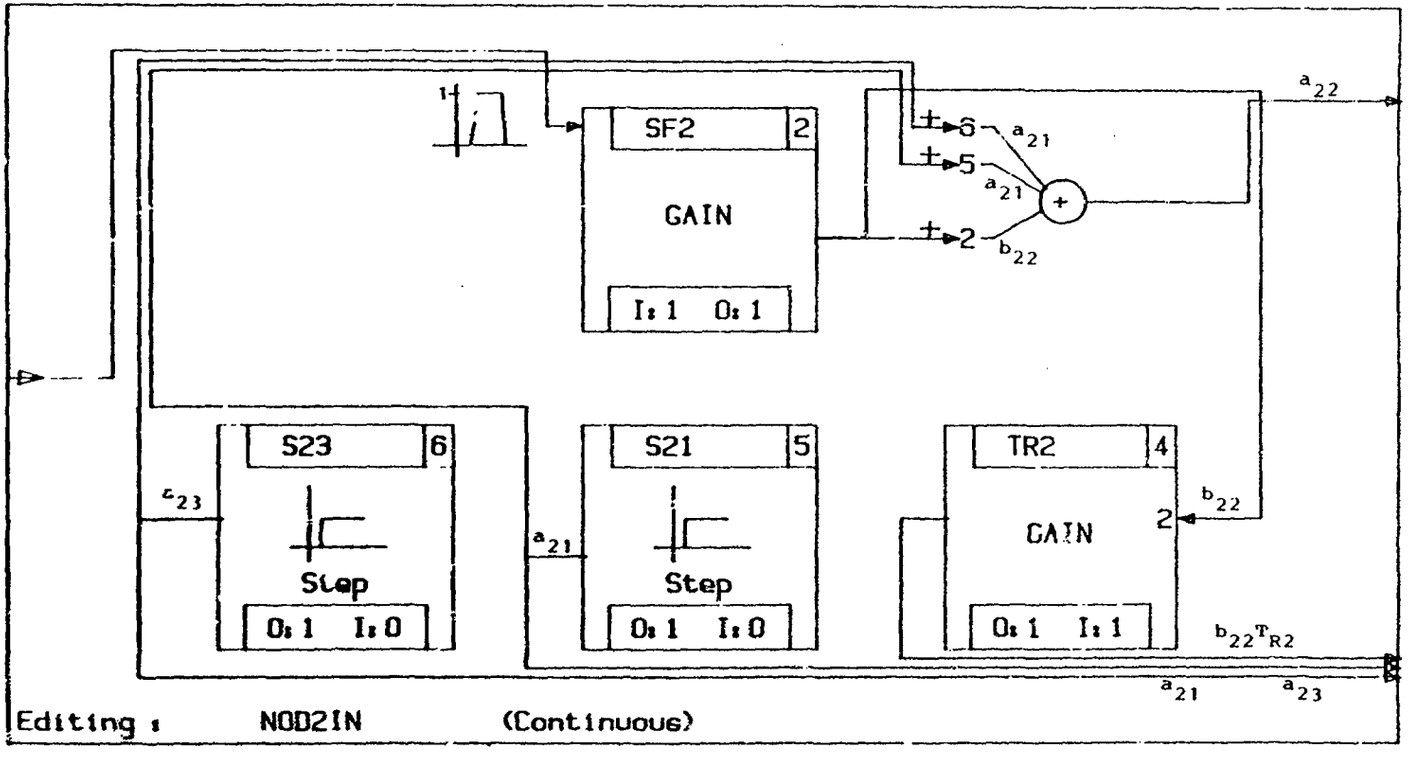
SF2
2
GAIN
I: 1 O: 1
6
5
2
a21
a21
b22
a22
S23
6
Step
O: 1 I: 0
S21
5
Step
O: 1 I: 0
TR2
4
GAIN
2
O: 1 I: 1
b22
b22TR2
a21
a23
Editing : NOD2IN (Continuous)

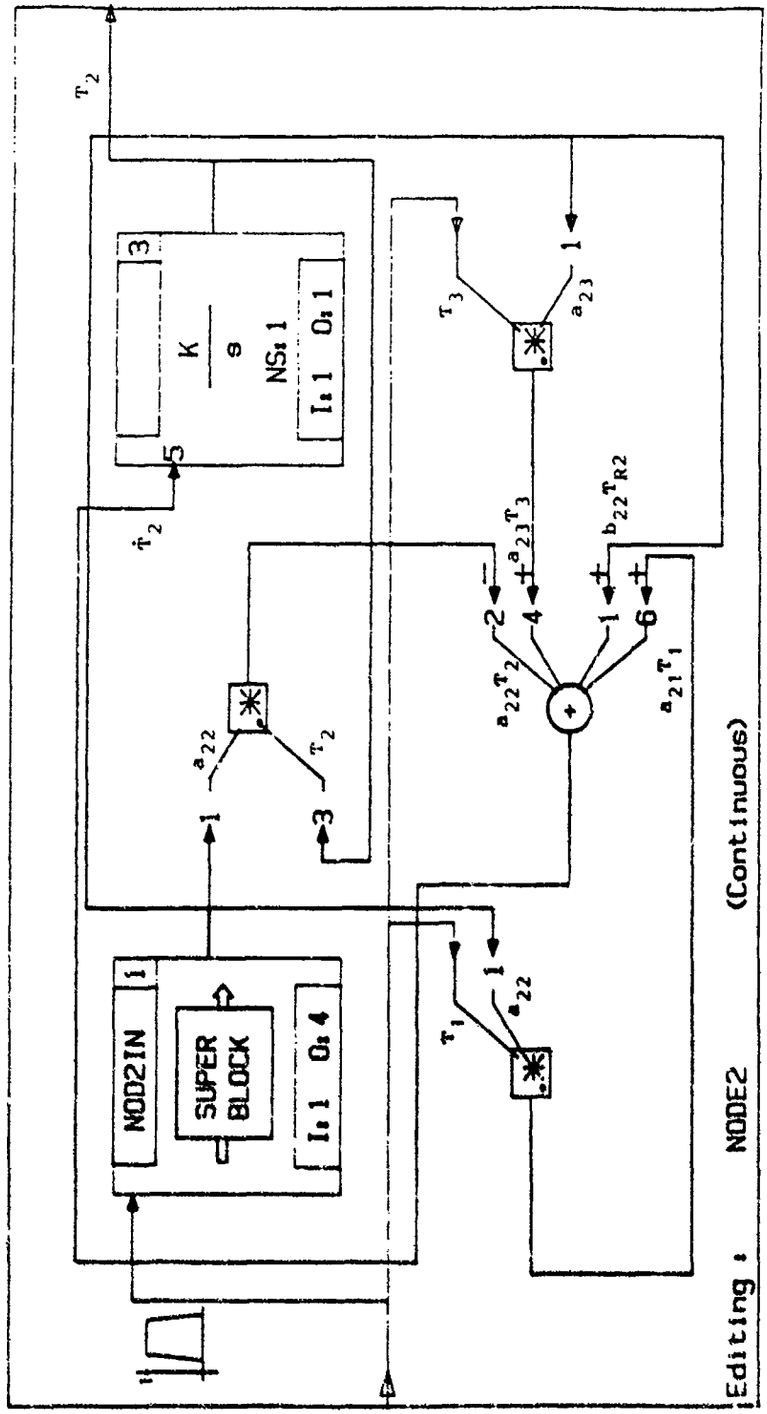
Editing : NODE2 (Continuous)
NOD2IN
SUPER BLOCK
I: 1 O: 4
K
s
NS: 1
I: 1 O: 1
T_2
T_3
T_1
a_{22}
a_{23}
$a_{22}T_2$
$a_{23}T_3$
$b_{22}T_{R2}$
$a_{21}T_1$

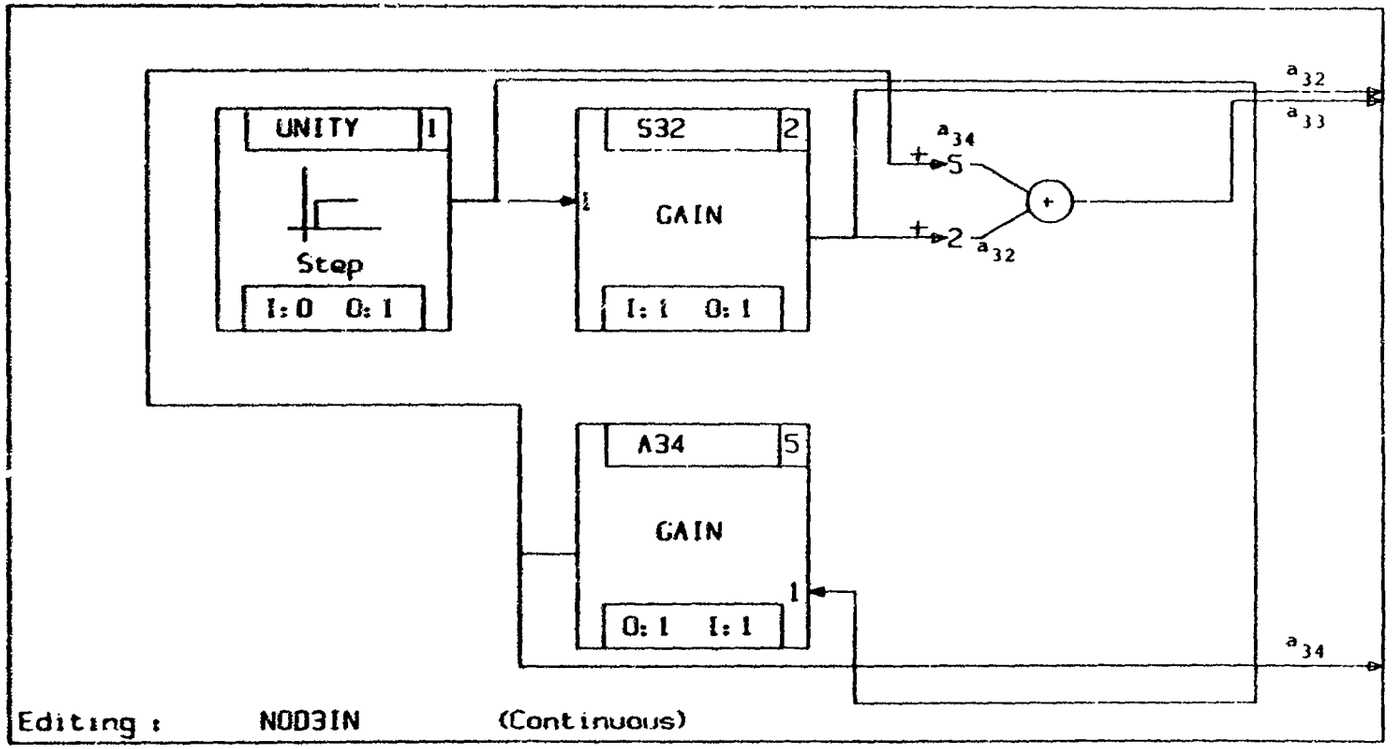
UNITY
1
Step
I:0 O:1
S32
2
GAIN
I:1 O:1
A34
5
GAIN
1
O:1 I:1
a34
5
2
a32
a32
a33
a34
Editing : NOD3IN (Continuous)

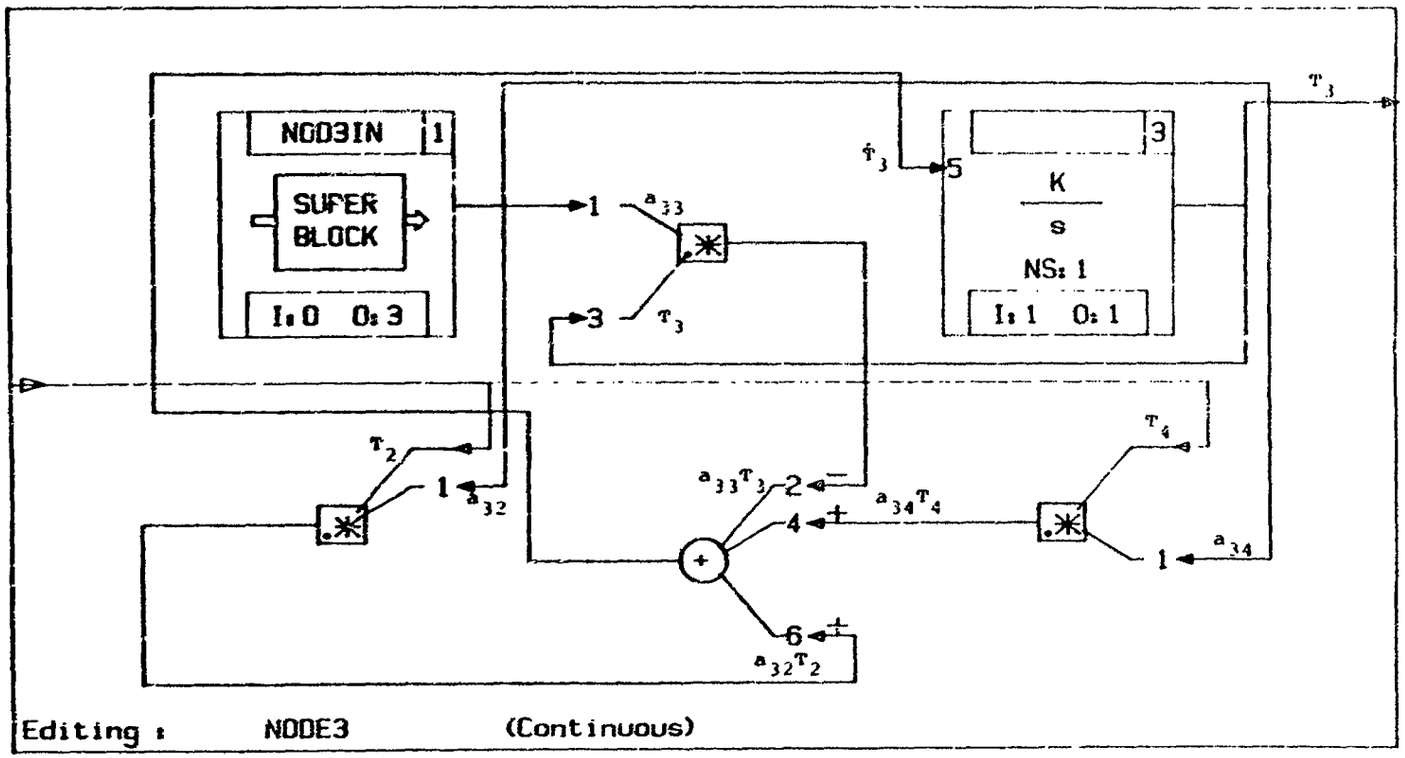
NOD3IN
1
SUPER BLOCK
I:0 O:3
1
3
a_{33}
T_3
$\dot{T}_3$
5
3
K
s
NS: 1
I:1 O:1
T_3
T_2
1
a_{32}
$a_{33}T_3$
2
4
$a_{34}T_4$
T_4
1
a_{34}
6
$a_{32}T_2$
Editing : NODE3 (Continuous)

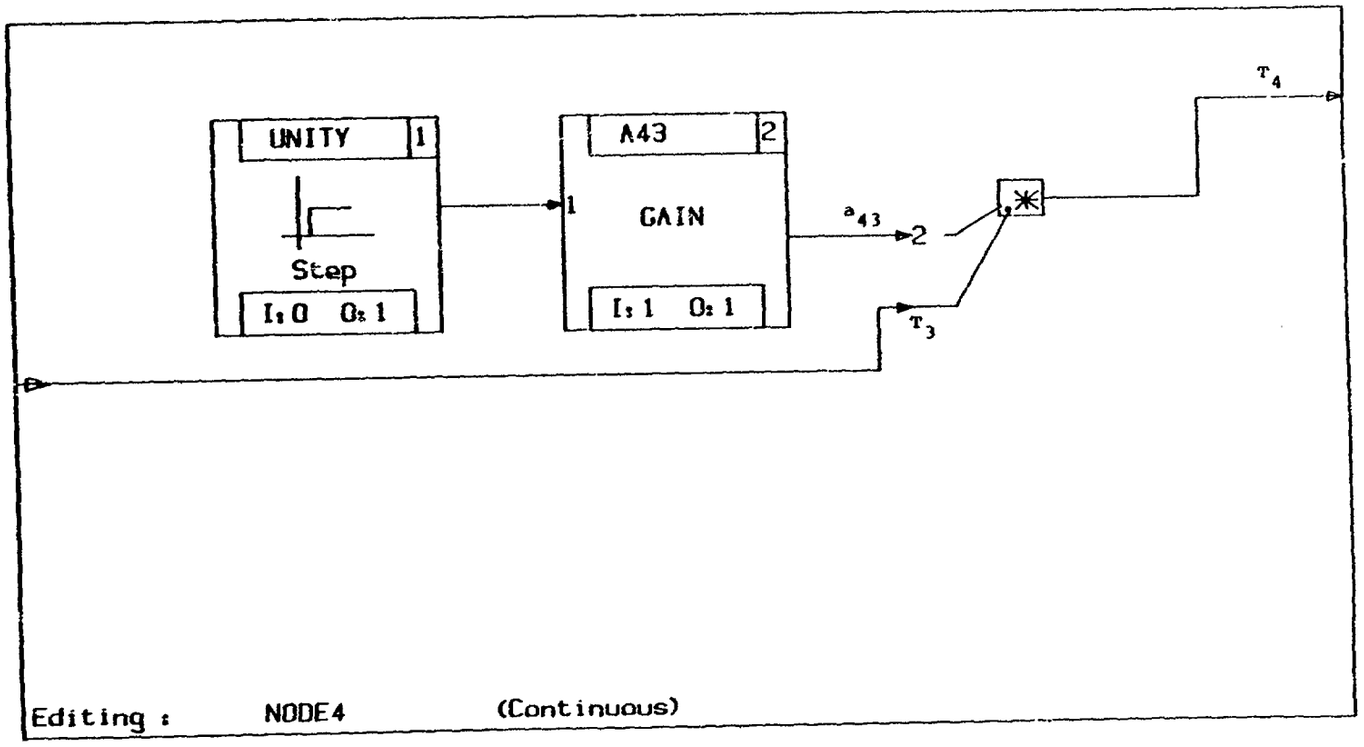
UNITY
1
Step
I: 0 O: 1
A43
2
1
GAIN
I: 1 O: 1
a43
2
T4
T3
Editing : NODE4 (Continuous)

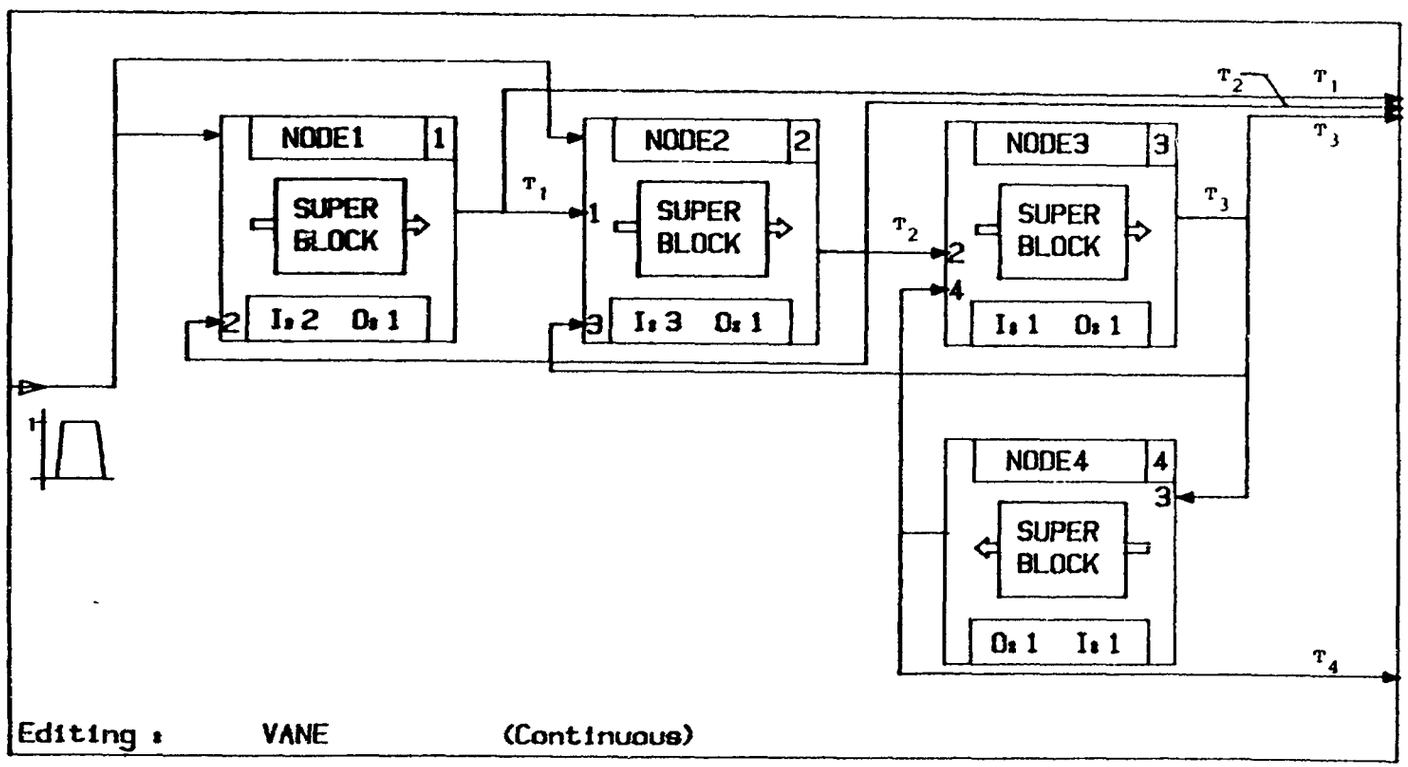
NODE1
1
SUPER BLOCK
I: 2 O: 1
NODE2
2
SUPER BLOCK
I: 3 O: 1
NODE3
3
SUPER BLOCK
I: 1 O: 1
NODE4
4
SUPER BLOCK
O: 1 I: 1
T1
T2
T3
T4
Editing : VANE (Continuous)

APPENDIX C

NWC TEST FIRING PARAMETERS

	Event(2)	Event (6)
Propellant	0% AL HTPB	18% AL HTPB
Molecular Weight	26.1	30.95
K =	1.210	1.145
C* =	4930 ft/sec	5175 ft/sec
C_d =	.934	.934
Burn rate Coefficient =	.05703 in/sec	.00807 in/sec
Burn rate exponent =	.28063	.54777
Ambient Conditions	70° F, 13.7 PSIA	70° F, 13.7 PSIA
Propellant Mass =	6.17 lbm	6.63 lbm
Propellant Density =	.06185 lbm/in^3	.06671 lbm/in^3
Initial Throat Area =	.14750 in^2	.26210 in^2
Post-fire Throat Area=	.15135 in^2	.26558 in^2
Max Pressure =	2286.8 PSI	1078.5 PSI
Max Thrust =	514 lbf	420 lbf
Total Impulse =	1535 lb-sec	1667 lb-sec
ISP =	248.8 sec	251.4 sec
Exit Dia =	1.8125"	1.815"
Max Exit Pressure =	12.3 PSI	14.8 PSI

REFERENCES

1. Nunn, R. H. and M. D. Kelleher, Jet Vane Heat Transfer Modeling, Naval Postgraduate School, Monterey, California, 1986.

2. National Aeronautics and Space Administration, Solid Rocket Thrust Vector Control, NASA SP-8114, Lewis Research Center, Cleveland Ohio, December 1974.

3. Kampa, D., A. Weiss, R. H. Schmucker, Material Problems in Jet Vane Thrust Vector Control Systems, AGARD-CP-259.

4. Wirtz, D. P., Preliminary Design and Performance Estimate of a Jet Vane Attachment in a Rocket Nozzle, Internal Memorandum 45701/DPW:cad, Reg. 45701-242-73, Naval Weapons Center, California, 4 June 1973.

5. Nunn, R. H., Modeling of Jet Vane Heat-Transfer Characteristics and Simulation of Thermal Response, Report to the TTCP Panel W4 (Propulsion Technology) Key Technical Area 9, Naval Postgraduate School, Monterey, California, 1987.

6. Holman, J. P. Heat Transfer, 6th ed., McGraw-Hill Book Co., New York, 1986.

7. Danielson, A. O., Aerodynamic Loading and Stress Analysis of a Retractable Jet Vane, Internal Memorandum, No. 5216-3273/r1387.

8. Nunn, R. H., TVC Jet Vane Thermal Modeling Using Parametric System Identification, Naval Postgraduate School, Monterey, California, March 1988.

9. Turbulent Flows and Heat Transfer, ed. C. C. Lin, v. 5, High Speed Aeronautics and Jet Propulsion, Princeton University Press, 1959.

10. Ziebland, H. and Parkinson, R. C., Heat Transfer in Rocket Engines, AGARD-AG-148-71, AGARD, September 1971.

11. White, F. M., Fluid Mechanics, 2nd ed., McGraw-Hill Book Co., New York, 1986.

12. International Business Machines Corporation Program Number 5789-PXJ, Dynamic Simulation Language/VS Language Reference Manual, June 1984.

13. Integrated Systems Inc., "SYSTEM_BUILD/PC User's Guide", Palo Alto, California, 1985.

14. Integrated Systems Inc., "MATRIXx/PC User's Guide", Palo Alto, California, 1985.

15. Integrated Systems Inc., "SYSTEM ID/PC User's Guide", Palo Alto, California, 1986.

INITIAL DISTRIBUTION LIST

		No. Copies
1.	Defense Technical Information Center Cameron Station Alexandria, Virginia 22304-6145	2
2.	Library, Code 0142 Naval Postgraduate School Monterey, California 93943-5002	2
3.	Chairman, Code 69 Mechanical Engineering Department Naval Postgraduate School Monterey, California 93943-5002	1
4.	Professor R. H. Nunn, Code 69Nn Mechanical Engineering Department Naval Postgraduate School Monterey, California 93943-5002	5
5.	LT Mark Hatzenbuehler Puget Sound Naval Shipyard Bremerton, Washington 98314-5000	3
6.	Surface Combatants Vertical Launching Systems Group, PMS 410 Naval Sea Systems Command Washington, D. C. 20362-5101	1
7.	Surface-To-Surface Weapons System Group SEA 62Y Naval Sea Systems Command Washington, D. C. 20362-5101	1
8.	Surface MIssile Weapons System Subgroup SEA 62Z Naval Sea Systems Command Washington, D. C. 20362-5101	1
9.	Mr. Arne Danielson, Code 32731 Naval Weapons Center China Lake, California 93555-5000	2